Aus dem Fachbereich Medizin
der Johann Wolfgang Goethe-Universität
Frankfurt am Main

betreut am
Zentrum der Molekularen Medizin
Institut für Kardiovaskuläre Regeneration
Direktorin: Prof. Dr. Stefanie Dimmeler

The role of *RGS5* downregulation in pericytes of the aging heart

Dissertation
zur Erlangung des Doktorgrades der Medizin
des Fachbereichs Medizin
der Johann Wolfgang Goethe-Universität
Frankfurt am Main

vorgelegt von
Jessica Neitz

aus Dillenburg

Frankfurt am Main, 2022

Dekan:	Prof. Dr. Stefan Zeuzem
Referentin:	Prof. Dr. Stefanie Dimmeler
Korreferent:	PD Dr. Matthias Leisegang
Tag der mündlichen Prüfung:	26.01.2023

Contents

List of Figures

List of Tables

Abbreviations

Actb	Actin beta
AT-1	Angiotensin II type 1
BBB	Blood brain barrier
BSA	Bovine serum albumin
C3	Complement component 3
CAD	Coronary artery disease
CCA	Canonical-correlation analysis
Ccl8	Chemokine C-C motif ligand 8
cDNA	Complementary DNA
CNS	Central nervous system
CO_2	Carbon dioxide
Col1a1	Collagen type I alpha 1 chain
Col5a2	Collagen type V alpha 2 chain
Cspg4	Chondroitin sulfate proteoglycan 4
CVD	Cardiovascular disease
DEG	Differentially expressed genes
DiI-Ac-LDL	DiI acetylated low density lipoprotein
Dmd	Dystrophin
DMEM	Dulbecco's Modified Eagle's Medium
DMSO	Dimethylsulfoxid
DNA	Deoxyribonucleic acid
dNTP	Deoxyribonucleoside triphosphate
DPBS	Dulbecco's Phosphate-Buffered Saline
EBM	Endothelial cell growth basal medium
EDG-1	Endothelial differentiation gene 1
EGM	Endothelial cell growth medium
ET-A	Type A endothelin

FACS	Fluorescence-activated cell sorting
FBS	Fetal bovine serum
FC	False change
Fgf13	Fibroblast growth factor 13
FITC	Fluorescein isothiocyanate
Fyttd1	Forty-two-three domain containing 1
GAPDH	Glyceraldehyde 3-phosphate dehydrogenase
GDP	Guanosine diphosphate
GFP	Green fluorescent protein
GO	Gene ontology
GPCR	G protein-coupled receptors
GRCm38	Genome Reference Consortium Mouse Build 38
GTP	Guanosine triphosphate
H_2O_2	Hydrogen peroxide
hBVP	Human brain vascular pericytes
HUVEC	Human umbilical vein endothelial cells
Map2k1	Mitogen-activated protein kinase kinase 1
MAPK	Mitogen-activated protein kinase
$MgCl_2$	Magnesium chloride hexahydrate
MMC	Microvascular mural cells
mRNA	Messenger RNA
MTT	3-(4,5-dimethylthiazol-2-yl)-2,5-diphenyl tetrazolium bromide
NADH	Nicotinamide adenine dinucleotide
Nexn	Nexilin
NG2	Neural/glial antigen 2
NO	Nitric oxide
NOTCH3	Neurogenic locus notch homolog protein 3
ns	Not significant
OD	Optic density

p.t.	Post transfection
PCR	Polymerase chain reaction
PDGFB	Platelet-derived growth factor subunit B
PDGFR	Platelet-derived growth factor receptor
PDGFRB	Platelet-derived growth factor receptor beta
Plcl1	Phospholipase C like 1
PVP	Polyvinylpyrrolidone
RGS5	Regulator of G protein signaling 5
RhoA	Ras homolog family member A
RNA	Ribonucleic acid
Rora	Retinoid acid receptor-related orphan receptor alpha
ROS	Radical oxygen species
RPLP0	Ribosomal protein lateral stalk subunit P0
rpm	Rotations per minute
RT-qPCR	Real time quantitative PCR
SEM	Standard errow of the mean
siRNA	Small interfering ribonucleic acid
snRNAseq	Single-nucleus RNA-sequencing
Stat3	Signal transducer and activator of transcription 3
Sulf1	Sulfatase 1
Tead1	TEA domain transcription factor 1
TEF1	Transcriptional enhancer factor 1 (TEF-1)
tSNE	t-Distributed Stochastic Neighbor Embedding
UIF	UAP56-Interacting Factor
UMI	Unique molecular identifier
VEGF	Vascular endothelial growth factor
vSMC	Vascular smooth muscle cells
Vtn	Vitronectin
α-SMA	Alpha-smooth muscle actin

1 Introduction

1.1 The cardiovascular system

1.1.1 Structure of heart and vasculature

The cardiovascular system provides the transport of oxygen and nutrients to the peripheral tissues of the organism. It is formed by the pulmonary circulation, which transports unoxygenated blood from the heart to the lungs, and the systemic circulation, which transports the oxygenated blood further into the organs of the body (Figure 1). The heart is the central organ of these two circuits and consists of a right and a left heart, which function as a pump for the pulmonary and systemic circulation, respectively. Both, the right and the left heart, are composed of an atrium and a ventricle. The atria and ventricles are separated by the cardiac valves, the triscupid valve on the right side and the mitral valve on the left side. These structures enable the blood to flow in one direction, avoiding reflux, from the atria to the ventricles and then to the arteries, the outgoing vessels of the heart. The transition of the ventricles into the truncus pulmonalis and the aorta, as the outgoing vessels of the heart, is also regulated by valves, the pulmonary valve on the right side and the aortic valve on the left side.[1] The main artery leaving the heart is the aorta that branches into smaller arteries and arterioles as its course guides into the different organs. Finally, arterioles lead to the capillary bed where the gas and nutrient exchange occurs. The capillaries merge into the venules that further merge into the larger veins that finally drain back into the heart via the vena cava.

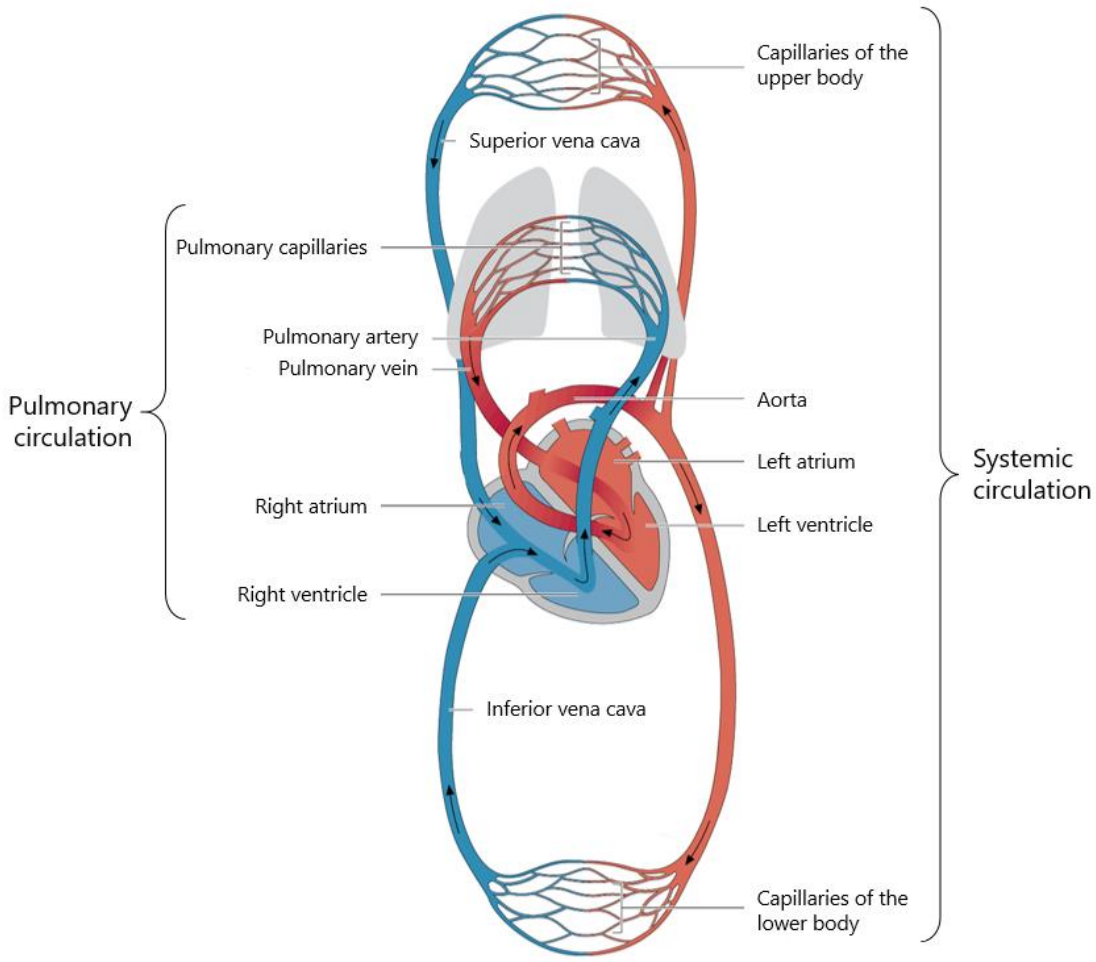

Figure 1: Structure of the circulatory system

The heart is the central pump of the pulmonary and systemic circulation of the body. The pulmonary circulation ensures the oxygenation of blood in the lungs which is then transported to the tissues of the body by the systemic circulation. Vessels that lead from the heart are named arteries. They end in the capillaries forming the terminal vascular bed, where gas and nutrient exchange and removal of metabolic products takes place. Veins are the vessels that drain the blood back to the heart.

Figure modified from Aumüller et al. 2010.[2]

The heart pumps blood into the arteries with high pressure, and thus, arteries present a thicker wall layer. The structure of the wall layers differs between arteries of the elastic and muscular type. In general, the arterial wall consists of three layers; the tunica intima, an inner layer of endothelial cells that is also known as endothelium, the tunica media, which is made up of smooth muscle cells, and the

tunica externa, also known as tunica adventitia, a layer of connective tissue that consists mainly of fibroblasts and collagen filaments. In contrast, veins show of a thinner wall layer as they are located in the low pressure system. The terminal vascular bed, also known as the microcirculation connects the arterial and venous system. This consists of arterioles, postcapillary venules, collecting venules and capillaries. Capillaries are the smallest component of the vascular system and consist only of an endothelium layer, a basal lamina and pericytes. The thin layer of the capillary wall and the slow flow velocity of the blood through these vessels ensures the correct exchange of gas and nutrients. Capillaries are also relevant for the removal of carbon dioxide (CO_2), as well as metabolic and toxic products (Figure 2).[3]

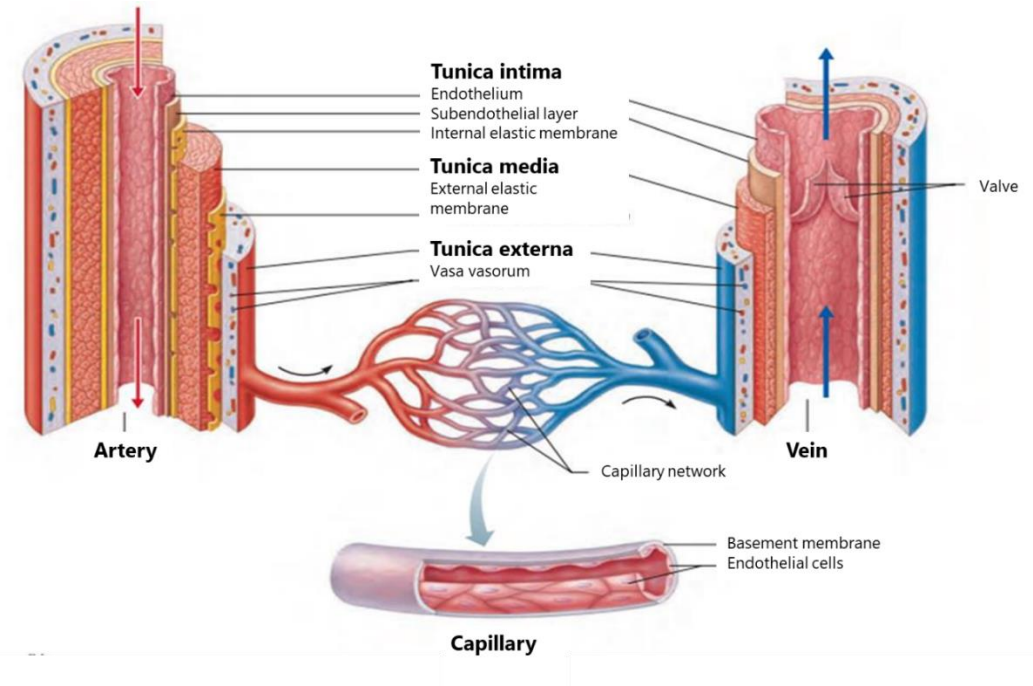

Figure 2: Blood vessel structures

Arteries, veins and capillaries differ in the structure of their wall layers. Both, arteries and veins are formed out of three layers; Tunica intima, tunica media and tunica adventitia. Arteries, located in the high pressure system, consist of thicker wall layers separated by elastic membranes. Capillaries are the smallest vessels of the body and consist only of a layer of endothelial cells with surrounding pericytes.

Figure modified from Marieb et al. 2010.[4]

Similar to the structure of the vessels, the heart also consists of different wall layers. As the inner endothelial layer, the endocardium covers all structures of the heart and is surrounded by subendothelial connective tissue. Underneath lies the myocardium, the main cardiac muscle tissue formed by cardiomyocytes. It is covered by an outer serous layer of mesothelium, called epicardium, and a subserous connective tissue layer. The heart is enclosed by the pericardium, which ensures the mobility of the heart through the fluid-filled pericardial cavity.[5]

1.1.2 Vascularisation of the heart

To perform their individual functions, the various organs of the body are supplied by specialized vascular and microvascular systems, with organotypically differentiated endothelial cells and mural cells.[6,7] Thereby, the perfusion of the heart muscle is ensured by an organ-specific vasculature, called coronary vasculature, formed by coronary arteries, arterioles, capillaries, venules and veins (Figure 3). The term originates from the Latin word corona for crown and refers to the crown-shaped course of the vessels that surround the heart muscle.

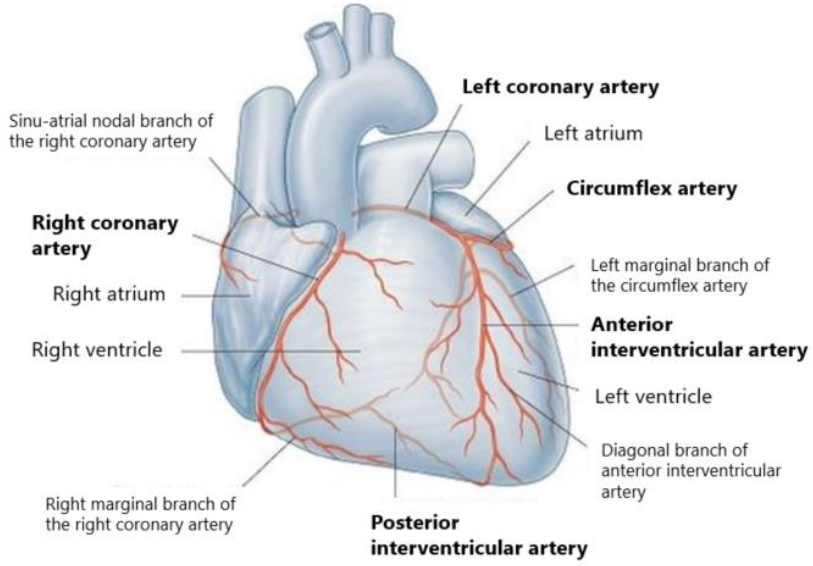

Figure 3: Structure of the coronary artery system

The organ-specific vasculature of the heart is known as the coronary system. Coronary arteries ensure the blood inflow of the heart muscle, the myocardium.

Figure modified from Drake et al. 2010.[8]

The right and left coronary artery originate directly from the ascending aorta and penetrate the myocardium from outside to supply the heart with oxygenated blood. The left coronary artery supplies the left atrium, the left ventricle with most of the ventricular septum, and a small part of the anterior wall of the right ventricle. In contrast, the right coronary artery supplies the right atrium, the right ventricle, the posterior third of the ventricular septum and some parts of the posterior wall of the left ventricle.

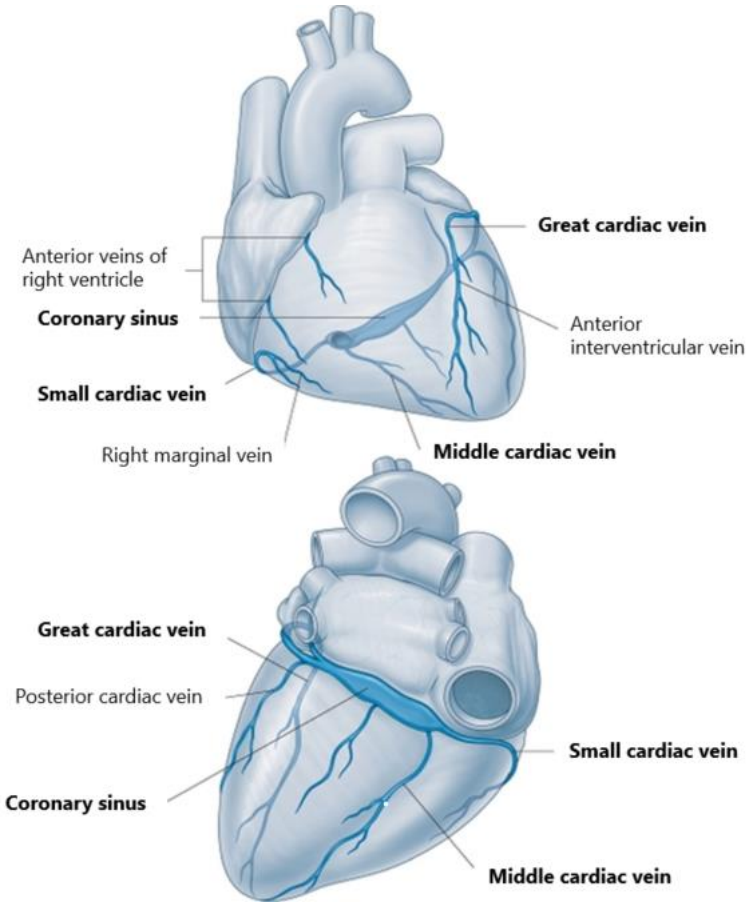

Figure 4: Structure of the coronary venous system

The venous drainage of the heart functions through the coronary sinus that obtains blood from the three main veins of the myocardium.

Figure modified from Drake et al. 2010.[8]

Most of the venous drainage in the heart is ensured by the coronary sinus that flows directly into the right atrium (Figure 4). The venous flow of this system is obtained from the great cardiac vein, the media cardiac vein, the small cardiac vein and the oblique vein of the left atrium. In addition to the system comprising the coronary sinus, veins of the heart surface, which are assigned to the transmural system, lead directly into the right atrium. A third system, which is summarized as endomural system, comprises the smallest cardiac veins, also known as Thebesius veins, of the inner heart muscle layer, which lead directly into the atria and ventricles.[2,9]

1.1.3 Cardiovascular aging

The phenotypes caused by cardiac aging have been described, but the molecular mechanisms that drive them are just beginning to be revealed and are not fully understood.

In general, aging can be described as a progressive process characterized by the impairment of cellular functions and that results in the development of age-related diseases caused by the accumulation of molecular damage.[10] There are a variety of mechanisms that induces this impairment, including genomic mutations caused by insufficient deoxyribonucleic acid (DNA) repair mechanisms, chromosomal telomere shortening, defective protein homeostasis and mitochondrial dysfunction with increased radical oxygen species (ROS) production. These mechanisms result in chronic cellular stress responses and cell damage associated with disturbed intracellular communication and functional decline of stem cells with reduced tissue repair.[11]

With regard to the cardiovascular system, aging is known to be the major risk factor for cardiovascular disease (CVD),[12] this includes atherosclerosis, hypertension, myocardial infarction and stroke.[13] In the western world, CVD is the leading cause of death.[14] The development of these diseases is based on various changes in the structure and the function of both the heart and the vasculature, previously reviewed in detail by Ferrari and colleagues.[15]

The aging vasculature is affected by structural changes of the vascular wall that lead to elongated vessels with an enlargement of the lumen and wall thickness, especially of the tunica intima and media.[16,17] In the aging arteries, endothelial cells show an irregular shape[18] with increased permeability and altered endothelial regulation of mural cells.[19] The dysfunction of endothelial cells during aging impairs the relaxation and anticoagulant functions of the vasculature.[19–21] Furthermore, an increased infiltration of immune cells has been observed, with intensified release of inflammatory substances, in aging arteries.[17] There have been described functional changes of the vasculature during aging. The vascular wall of the central arteries becomes stiffer with age[22] due to changes in the composition of collagen and elastin in the artery wall. Furthermore, the proliferation and tonus dysregulation of contractile vascular smooth muscle cells (vSMC) contribute to these vascular alterations.[17] These structural changes affect the Windkessel effect of the aorta[23] with an altered pulse wave velocity and a higher total peripheral resistance leading to the increased systolic pulse pressure described above.

There is evidence that the heart weight increases during aging due to hypertrophy of the left ventricle.[24] This hypertrophy could be caused by an increase of systolic pressure during the contraction phase of the heart and is associated with an increased risk for cardiovascular events, including myocardial infarction, heart failure, stroke, dementia or renal disease.[17] The chronic raise of systolic pressure

causes remodeling of the microvasculature in the heart and an increased wall thickness of arterioles with impaired perfusion of the myocardium.[15] In contrast to this, the pressure of the diastolic ejection phase is reduced in aged hearts. The diastolic pressure is crucial for maintaining the perfusion of the coronary arteries. Thus, age-related reduction in diastolic pressure is associated with increased development of coronary heart disease and myocardial ischemia in aging.[25,26] The macroscopic changes here described, reflect changes on the cellular level. Aged hearts present enlarged cardiomyocytes[27] and an increase of intercellular collagen connections.[28] Furthermore, aging induces the degeneration of sympathetic nerves in the heart. This degeneration is associated with functional changes in the heart like an altered responsiveness to catecholamine stimuli.[29]

Age-related alterations also occur in the microvasculature. An increased tone of the microvascular vessels causes remodeling processes characterized by enlargement of the vascular walls and endothelial dysfunction. The latter leads to effects on various vascular functions, including sprouting of new vessels, defined as angiogenesis, the regulation of vasodilation and inflammatory processes through increased expression of adhesion molecules affecting the migration of inflammatory cells.[30] One of the main causes of the alteration of the endothelium is the increased oxidative stress with exposure to ROS and changes in the nitric oxide (NO) homeostasis.[31] NO is a small signaling molecule released by the endothelial cells to regulate diverse physiological processes, including smooth muscle relaxation, vasodilatation and angiogenesis.[32] These changes also affect the aging process of the myocardium in the heart, but the exact impact on age-related disease of the cardiovascular system is not yet well understood.[30]

Other cell types of the microvasculature, namely vSMC and pericytes, are affected by these changes during aging. vSMC show an altered phenotype and impaired functionality leading to reorganization processes of the microvascular wall with

increased fibrosis.[33,34] The role of pericytes in the aging microvasculature has not been studied so far and will be the focus of this work.

1.2 Pericytes

1.2.1 Definition

In 1873, Charles-Marie Benjamin Rouget discovered a new type of perivascular mural cell around the capillary wall with the ability of contraction.[35] They were originally named Rouget cells, after the scientist that first described them, and only first named pericytes in 1923 by Zimmermann.[36] Zimmermann further developed the definition of these cells and described the pericytes as cells with a branched shape and cytoplasmatic extensions associated with the vSMC around the capillaries. He discovered that pericyte contraction is required for capillary permeability and set the basis for the research of pericyte physiology and their importance for the function of the vascular system.[37] Based on the current state of research, pericytes are defined as perivascular cells located in the basement membrane of capillaries, precapillary arterioles and postcapillary venules (Figure 5).[38] Their location and individual branch pattern along the vessel wall are relevant for the classification of pericyte subclasses.[39]

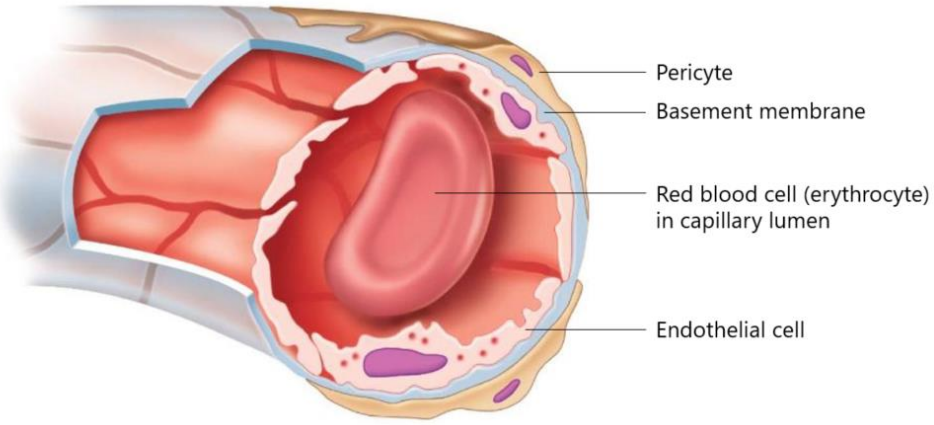

Figure 5: Pericytes as perivascular cells of the capillary system

Pericytes are besides endothelial cells involved in the construction of the capillaries as the smallest component of the vascular system. The two cell types are separated by a shared basement membrane.

Figure modified from Alcendor et al. 2019.[40]

Throughout the vasculature, pericytes acquire different phenotypes. These represent a phenotypical shift from pericytes to vSMC at the transition from capillaries to arterioles and venules (Figure 6). Pericytes surrounding capillaries present a round cell body with processes to enwrap the endothelial cell layer. Transitional cells at the precapillary side show a more pronounced network of cellular processes to encircle the endothelial cells, while postcapillary mural cells are characterized by slender processes with many branches and a flattened cell body. As for this transitional microvascular mural cells (MMC), the vSMC differ between the arterial and venous vascular bed. Arterial vSMC have a flattened and spindle-shaped body with few processes. The venous type of vSMC is characterized by a big and stellate shaped cell body with a high number of branching extensions.[41]

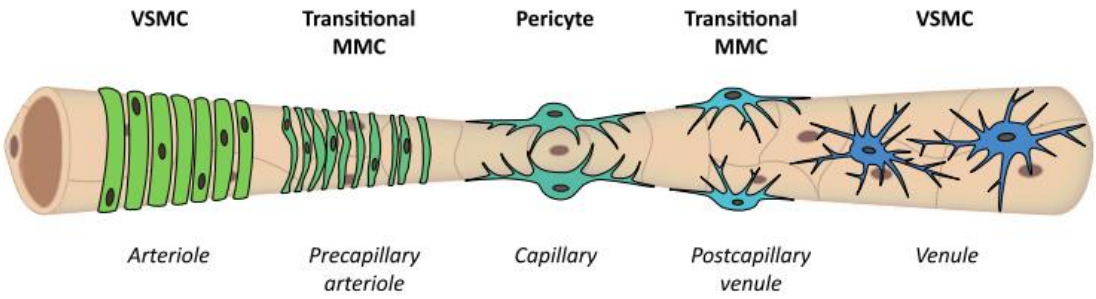

Figure 6: Phenotypical transition of pericytes in the microvasculature

Pericytes change their phenotypical properties at the transition of capillaries to precapillary arterioles and postcapillary venules. These transitional MMC represent an intermediate cell type between pericytes and vSMC.

Figure modified from Holm et al. 2018.[7]

Previous studies have shown that in different organs, pericyte acquire organ-specific functions.[7] For this reason, pericytes can receive different names in different organs, such as the mesangial cells of the renal glomeruli and the Ito-cells as perisinusoidal cells of the liver.[42,43] The organ-specificity of pericytes and other murals cells can be explained by the developmental origins of these cells. Regarding the coronary system, mural cells derive from epicardial mesothelium or from the endocardium through endothelial–mesenchymal transition.[44] There is evidence that pericytes serve as progenitor cells of coronary vSMC.[45] The specific origin of the mural cells of the coronary system provides an explanation for the increased susceptibility of this vascular bed to the development of diseases such as atherosclerosis.[46] Pericytes also show a close ontogenic relationship to fibroblasts and the possible transdifferentiation of mural cells of the vasculature into fibroblasts is still part of current research.[7,47]

For identification of pericytes and their distinction from other mural cell types, researchers use a list of different molecules that function as pericyte markers including alpha-smooth muscle actin (α-SMA), desmin, platelet-derived growth factor receptor beta (PDGFRB), aminopeptidase A and N (CD13) and neural/glial antigen 2 (NG2) proteoglycan. These molecules are expressed in a specific pattern depending on the corresponding vessel type and the location of pericytes in different vascular areas.[37,48]

1.2.2 Functions

Pericytes participate in the interaction between the different vascular cells that regulate the function of the vascular system. They are responsible for the stabilisation of the vascular wall and the control of the proliferation and maturation of endothelial cells. Also, through this interaction with the endothelial cells, pericytes regulate the permeability of the vascular wall. Pericytes are also

known for the contribution to the angiogenesis of capillaries.[37] Neural tissues, particularly brain and retina have the highest density of mural cells.[47] And thus, it has been a lot of research effort devoted to the study of mural cells in these vascular beds. Special functions of pericytes in the central nervous system (CNS) are especially the formation of growing vessels, the preservation of the blood brain barrier (BBB) and the control of immune cell migration inside the brain. By active relaxation, pericytes take part in capillary constriction and relaxation for controlling the blood flow.[48] In addition to this wide range of functions, cultured pericytes are known to have the potential of multipotent stem cells under hypoxic conditions with the ability to differentiate into cells of the neural and vascular lineage.[49] The study of pericytes as progenitors of various mesenchymal cells is the subject of current research.[50]

1.2.3 Pericytes in disease and aging

Pericytes are involved in the development of different pathological processes like ischemia, cerebrovascular dysfunctions, tumor growth and pericyte-specific genetic defects.[38] Furthermore, the development of diabetic retinopathy due to chronic hyperglycemia is accompanied by a characteristic loss of pericytes leading to reduced integrity of the vascular wall that makes the organism more prone to the formation of retinal microaneurysms and macula edemas.[47]. In tumors, pericytes differ in their appearance and expression pattern of cellular markers compared to normal pericytes. They contribute to the increased angiogenic formation of tumor vasculature.[47]

Pericytes also participate in the age-related changes of the microvasculature, with a thickening of the basement membrane and dilation of capillaries.[51] These alterations are associated with an impaired interaction between pericytes and endothelial cells and the loss of pericytes with reduced pericyte coverage of

capillaries described in the retina, leading to destabilisation of the vascular wall.[51,52] Further, morphologic changes have been described in aging pericytes with transition to a phenotype resembling that of arterial vSMC. This was associated with increased formation of adhesion contacts in the vascular wall.[51] The differentiation of pericytes to osteoblastic cells is also linked to the development of arterial calcifications leading to atherosclerosis.[53]

1.2.4 Role of pericytes in the cardiovascular system

Besides the endothelial cells, the pericytes of the myocardium form a large proportion of interstitial cells that are not assigned to the population of cardiomyocytes due to the highly developed capillary network. The role of pericytes in the heart and in aging capillaries of the myocardium is not yet understood. A loss of pericytes throughout the body is associated with malfunction of vessel development, the formation of microaneurysm and an increased incidence of cardiotoxic effects and cardiomyopathy. In the context of myocardial infarction, pericytes are relevant for the regulation of capillary permeability and participate in the signaling processes with immune cells in the inflammatory phase of the infarcted tissue. In addition, pericytes stabilize the infarct scar by covering the neoangiogenic vessels.[54]

Despite the progress made in research on pericytes, their exact role and the mechanisms by which pericytes are involved in the cardiovascular system and the aging process are not yet fully understood.

1.3 RGS5

1.3.1 Function

Regulator of G protein signaling 5 (RGS5) belongs to a family of regulatory signaling transduction proteins. These proteins negatively regulate the

heterotrimeric G proteins of G protein-coupled receptors (GPCR) that are relevant for the modulation of different biological processes. GPCRs include, among others, proteins that regulate cardiovascular functions by catecholamines. The transformation of guanosine triphosphate (GTP), bound to the α-unit of heterotrimeric G proteins, to inactive guanosine diphosphate (GDP) through the integrative GTPase activity of RGS proteins inhibits the subsequent signal transduction cascade (Figure 7).

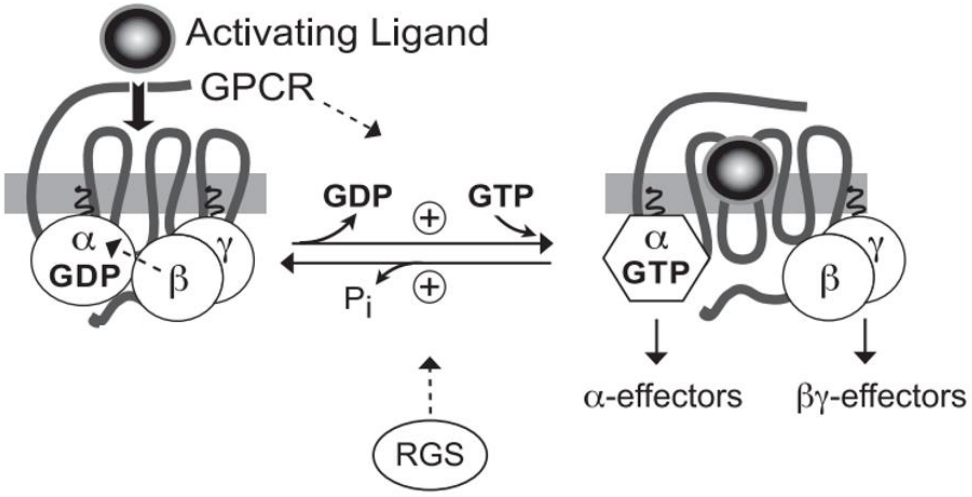

Figure 7: Molecular mechanism of the regulatory function of RGS proteins

RGS proteins are regulators of GPCRs. GPCRs are connected with heterotrimeric G-proteins that regulate subsequent signaling cascades. After binding of a receptor ligand, inactive GDP is released from the α-unit and exchanged with active GTP resulting in a dissociation of the subunits and the activation of signaling molecules. RGS proteins function in the acceleration of hydrolysis of GTP to GDP to inhibit the activation of downstream signaling pathways.

Figure modified from Kimple et al. 2011.[55]

RGS5 has a high affinity to G_i and G_q of heterotrimeric G proteins, defined as subtypes of the G protein α unit that are associated with specialized downstream signaling pathways to control different cellular functions. The regulation via RGS5 attenuates signaling pathways that are important for vascular processes and

development, such as signaling through endothelial differentiation gene 1 (EDG-1), angiotensin II type 1 (AT-1) and type A endothelin (ET-A) and platelet-derived growth factor receptor (PDGFR).[56–58]

1.3.2 Role of RGS5 in pericytes and the cardiovascular system

RGS5 is mainly expressed in pericytes and smooth muscle cells, and it has been defined as a molecular marker for these cell types.[59,60]

The role of RGS5 has been investigated in the past, mainly in the context of tumor vascularization and neoangiogenesis. RGS5 is highly upregulated in angiogenic pericytes in tumor vessels, wound healing and ovulation, indicating a correlation between RGS5 expression and vascular remodeling processes.[61] In vSMC, the expression of RGS5 appears to contribute to the angiogenesis of collateral arterioles.[62] RGS5 is also relevant for various cardiovascular diseases, including cardiac hypertrophy, myocardial infarction and atherosclerosis.[63–66] There is also a connection between RGS5 and the regulation of blood pressure.[67] The role of RGS5 in the aging pericytes has not been yet investigated.

2 Objectives

Aging is the main risk for the development of cardiovascular disease. The molecular mechanisms behind the age-related alterations in the vasculature, especially in the pericytes, remain undiscovered. Pericytes play a crucial role in the development and homeostasis of the vascular system. Recent studies have reported that pericytes are a very heterogeneous population that plays different roles and functions in different organs. The role of pericytes during disease and aging in the cardiovascular remains unclear. This work aims to unveil the molecular mechanisms responsible for pericyte aging in the heart and has the three following objectives:

1. Characterize the pericyte population in young and old hearts.
2. Analyse the gene expression signature of old and young pericytes to identify genes responsible for pericyte aging.
3. Investigate the biological function in pericytes of deregulated genes during cardiac aging.

3 Materials and Methods

3.1 Materials

Table 1: Equipment

Equipment	Company
Axiovert 100	Carl Zeiss (Oberkochen, Germany)
BioTek Synergy™ HT Multi-Detection Microplate Reader	BioTek (Winooski, VT, USA)
Comfort Fridge	Liebherr (Bulle FR, Switzerland)
Eppendorf Reference Pipettes 1000 µl, 100 µl, 10 µl	Eppendorf (Hamburg, Germany)
GeneAmp® PCR System 9700	Applied Biosystems (Foster City, CA, USA)
GloMax®-Multi Detection System	Promega (Madison, Wisconsin, USA)
KS 130 basic orbital shaker	IKA (Staufen, Germany)
Leica CM3050 S cryostate	Leica Biosystems (Wetzlar, Germany)
Leica SP8 inverted confocal microscope	Leica Biosystems (Wetzlar, Germany)
Micro 200R	Hettich (Kirchlengern, Germany)
Mini Star silverline	VWR International (Radnor, Pa, USA)
Multifuge3s	Heraeus (Hanau, Germany)
NanoDrop™ 2000 Spectrophotometer	Thermo Scientific (Karlsruhe, Germany)
New Brunswick™ Galaxy® 170 S CO2 Incubator	Eppendorf (Hamburg, Germany)
NucleoCounter	ChemoMetec (Allerod, Denmark)

Pipetboy acu 2 Pipette Controller	INTEGRA Biosciences (Zizers, Switzerland)
Plate centrifuge	STARLAB (Hamburg, Germany)
Premium NoFrost Freezer	Liebherr (Bulle FR, Switzerland)
SmartSpec Plus Spectrophotometer	Bio-Rad (Hercules, CA, USA)
Sterile Hood Herasafe	Heraeus (Hanau, Germany)
Vacuboy Hand Operator	INTEGRA Biosciences (Zizers, Switzerland)
ViiA 7 Real-Time PCR System	Applied Biosystems (Foster City, CA, USA)
Vortex Genie 2	Scientific Industries (Bohemia, NY, USA)

Table 2: Software and Web tools

Software	**Company**
BioRender	BioRender (Toronto, ON, Canada)
Enrichr	Ma'ayans Lab (Icahn School of Medicine at Mount Sinai)
Excel 2013	Microsoft Office
Gen5™ Software	BioTek (Winooski, VT, USA)
GraphPad Prism8 Software	GraphPad Software (San Diego, CA, USA)
NanoDrop 2000 Software	Thermo Scientific (Karlsruhe, Germany)
NIS-Elements Imaging Software	Nikon Instruments (Minato, Japan)
PANTHER Classification System	Gene Ontology Phylogenetic Annotation Project

Cell Ranger 2.1.1 Gene Expression Software	10X Genomics (Pleasanton, CA, USA)
Seurat 2.2.0 Software	Satijah Lab (New York City, NY, USA)
ViiA™ 7 Software	Applied Biosystems (Foster City, CA, USA)
Volocity Software	Quorum Technologies (Puslinch, Ontario, Canada)

Table 3: Consumables

Consumable	Company	Reference
10/20 µl RPT XL Graduated Filter Tip (Sterile)	STARLAB (Hamburg, Germany)	S1180-3710
100 µl RPT Bevelled Filter Tip (Sterile)	STARLAB (Hamburg, Germany)	S1180-1840
1000 µl RPT XL Graduated Filter Tip (Sterile)	STARLAB (Hamburg, Germany)	S1182-1730
Amicon Ultra-15, PLHK Ultracel-PL Membran, 100 kDa	Merck Millipore (Burlington, MA, USA)	UFC910024
Cell culture dish, 60/15 mm, CELLSTAR® TC, STERILE	Greiner bio-one (Kremsmünster, Austria)	628160

Cell culture flask, 250 ml, 75 cm^2	Greiner bio-one (Kremsmünster, Austria)	658170
Cell culture flask, 50 ml, 25 cm^2	Greiner bio-one (Kremsmünster, Austria)	690160
Cell culture flask, 550 ml, 175 cm^2	Greiner bio-one (Kremsmünster, Austria)	660160
Cell culture multiwell plate, 12 well, clear, CELLSTAR®	Greiner bio-one (Kremsmünster, Austria)	665180
Cell culture multiwell plate, 24 well, clear, CELLSTAR®	Greiner bio-one (Kremsmünster, Austria)	662160
Cell culture multiwell plate, 48 well, clear, CELLSTAR®	Greiner bio-one (Kremsmünster, Austria)	677180
CELLSTAR® Centrifuge tubes 15 ml, sterile	Greiner bio-one (Kremsmünster, Austria)	188271
CELLSTAR® Centrifuge tubes 50 ml, sterile	Greiner bio-one (Kremsmünster, Austria)	227261
Corning® Costar® Stripette 10 ml	Corning (New York, USA)	CLS4488
Corning® Costar® Stripette 25 ml	Corning (New York, USA)	CLS4487

Corning® Costar® Stripette 5 ml	Corning (New York, USA)	CLS4487
Corning® cryogenic vials, internal thread	Corning (New York, USA)	8672
Cuvette semi-micro 1.6 ml, acrylic	Sarstedt (Nümbrecht, Germany)	67.740
MicroAmp™ EnduraPlate™ Optical 384-Well Blue Reaction Plates with Barcode	Applied Biosystems (Foster City, CA, USA)	4483320
MicroAmp™ Optical Adhesive Film	Applied Biosystems (Foster City, CA, USA)	4311971
Microplate, 96 well, f-bottom µCLEAR®, black, sterile	Greiner bio-one (Kremsmünster, Austria)	655097
PARAFILM®M laboratory film	Sigma-Aldrich (Steinheim, Germany)	P6543
Safe Lock Tubes 1.5 ml	Eppendorf (Hamburg, Germany)	0030120086
Safe Lock Tubes 2.0 ml	Eppendorf (Hamburg, Germany)	0030120094
Thincert cell culture insert for 24 well plates, sterile, transparent membrane, pore diameter: 1 µm	Greiner bio-one (Kremsmünster, Austria)	662610

Table 4: Chemicals

Chemical	Company	Reference
3-(4,5-dimethylthiazol-2-yl)-2,5-diphenyl tetrazolium bromide (MTT)	Invitrogen (Carlsbad, CA, USA)	M6494
Chloroform	J.T. Baker (Phillipsburg, NJ, USA)	15598554
Dimethylsulfoxid (DMSO)	Sigma-Aldrich (Steinheim, Germany)	D4540
Deoxyribonucleoside triphosphate (dNTP) Mix 100 mM	Applied Biosystems (Foster City, CA, USA)	362271
Fast SYBR Green Master Mix	Applied Biosystems (Foster City, CA, USA)	4385612
Fibronectin human plasma	Sigma-Aldrich (Steinheim, Germany)	F0895-5MG
Fluorescein isothiocyanate (FITC)-Dextran	Sigma-Aldrich (Steinheim, Germany)	FD70S
Fluoromount-G™	Invitrogen (Carlsbad, CA, USA)	00-4958-02

Gelatin (2% in water)	Sigma-Aldrich (Steinheim, Germany)	G1393
Gelatin from porcine skin	Sigma-Aldrich (Steinheim, Germany)	G1890
GeneJuice® Transfection Reagent	Sigma-Aldrich (Steinheim, Germany)	70967
Histamine	Sigma-Aldrich (Steinheim, Germany)	H7125
Lipofectamine™ RNAiMAX Reagent	Invitrogen (Carlsbad, CA, USA)	13778150
Human Dil acetylated low density lipoprotein (DiI-Ac-LDL)	Invitrogen (Carlsbad, CA, USA)	L3484
M-MLV RT Buffer	Invitrogen (Carlsbad, CA, USA)	18057-018
Poly-L-lysine solution 0.01%, sterile-filtered, 30,000-70,000 kDa	Sigma-Aldrich (Steinheim, Germany)	P4707
Polyvinylpyrrolidone (PVP)	Sigma-Aldrich (Steinheim, Germany)	P5288
QIAzol® Lysis Reagent	Qiagen (Hilden, Germany)	79306

Random Hexamer Primer	Thermo Scientific (Karlsruhe, Germany)	SO142
RNase-Inhibitor (2,000 U, 20 U/µl)	Applied Biosystems (Foster City, CA, USA)	N8080119
ROTI® Histofix 4%	Carl Roth (Karlsruhe, Germany)	P087
Sucrose	Sigma-Aldrich (Steinheim, Germany)	S0389
SuperScript™ III Reverse Transcriptase	Invitrogen (Carlsbad, CA, USA)	18080044
UltraPure™ DNase/RNase-Free Distilled Water	Invitrogen (Carlsbad, CA, USA)	10977015

Table 5: Enzymes

Enzyme	Company	Reference
Trypsin 2.5% (10X)	Gibco Life Technologies (Darmstadt, Germany)	15090046

Table 6: Kits

Kit	Company	Reference
EndoFree Plasmid Maxi Kit	Qiagen (Hilden, Germany)	12362

miRNEasy Mini Kit	Qiagen (Hilden, Germany)	74104
RNase-Free DNase Set	Qiagen (Hilden, Germany)	79254

Table 7: Cell culture media

Medium	Company	Reference
Dulbecco's Modified Eagle's Medium (DMEM) (high glucose, [+] L-Glutamin, [+] Sodium-Pyruvat)	Gibco Life Technologies (Darmstadt, Germany)	D5671
Endothelial cell growth basal medium (EBM)	Lonza (Basel, Switzerland)	CC-3121
Matrigel Matrix Basement Membrane growth factor reduced	Gibco Life Technologies (Darmstadt, Germany)	354230
OPTI-MEM I (1X) Reduced serum medium	Gibco Life Technologies (Darmstadt, Germany)	31985070

Table 8: Cell culture media supplements

Supplement	Company	Reference

Endothelial cell growth medium (EGM) SingleQuots™ Kit	Lonza (Basel, Switzerland)	CC-4133
Fetal bovine serum (FBS), Qualified	Gibco Life Technologies (Darmstadt, Germany)	10270-106
Penicillin-Streptomycin	Roche (Mannheim, Germany)	11074440001

Table 9: Buffers

Buffer	Company	Reference
Dulbecco's Phosphate- Buffered Saline (DPBS (1X) [-]$CaCl_2$ [-]$MgCl_2$)	Gibco Life Technologies (Darmstadt, Germany)	14190-094

Table 10: Primary antibodies

Primary antibody	Company	Reference
Fluorescein labeled Griffonia (Bandeiraea) Simplicifolia Lectin I (GSL I, BSL I)	Vector Laboratories (Lörrach, Germany)	FL-1101
Rgs5 Polyclonal Antibody	Invitrogen (Carlsbad, CA, USA)	PA5-75560

Table 11: Secondary antibodies

Secondary Antibody	Company	Reference
Hoechst 33342 Staining Dye Solution	Abcam (Cambridge, UK)	ab228551
Polyclonal Goat Anti-Rabbit Immunoglobulins/ Biotinylated	Dako (Hamburg, Germany)	E0432

Table 12: Staining materials

Material	Company	Reference
Menzel™ Microscope Coverslips 24x60 mm	Thermo Scientific (Karlsruhe, Germany)	15747592
SuperFrost Plus™ Adhesion slides	Thermo Scientific (Karlsruhe, Germany)	J1800AMNZ

Table 13: Staining reagents

Reagent	Company	Reference
Bovine serum albumin (BSA)	Sigma-Aldrich (Steinheim, Germany)	A7030
Dako Fluorescence Mounting Medium	Dako (Hamburg, Germany)	S3023
Hydrogen peroxide (H_2O_2), 30%	Carl Roth (Karlsruhe, Germany)	8070
Methanol	Fisher Chemical	11976961

Magnesium chloride hexahydrate ($MgCl_2$)	Carl Roth (Karlsruhe, Germany)	2189.1
Normal donkey serum	Jackson ImmunoResearch Laboratories (West Grove, Pa, USA)	017-000-121
tri-Sodium citrate dihydrate	Carl Roth (Karlsruhe, Germany)	3580.1
Triton X-100	Sigma-Aldrich (Steinheim, Germany)	T8787
TSA Cyanine 3 Tyramide Reagent Pack	Perkin Elmer (Waltham, MA, USA)	SAT704A
VECTASTAIN® Elite® ABC HRP Kit (Peroxidase, Standard)	Vector Laboratories (Lörrach, Germany)	PK-6100

Table 14: Human primers for RT-qPCR

All primers were purchased from Sigma-Aldrich (Steinheim, Germany).

Primer	**Forward sequence (5'-3')**	**Reverse sequence (5’-3’)**
Collagen type I alpha 1 chain *(COL1A1)*	CCAACCGAACATGACCAA	GGCAGAAAGGGACTTACC
Glyceraldehyde 3-phosphate	ATGGAAATCCCATCACCATCTT	CGCCCCACTTGATTTTGG

dehydrogenase *(GAPDH)*		
Neurogenic locus notch homolog protein 3 (*NOTCH3*)	CGCGTGGCTTCTTTCTACTG	AGATAGCATCCTCGTGGCAG
PDGFRB	AGCACCTTCGTTCTGACCTG	TATTCTCCCGTGTCTAGCCCA
Ribosomal protein lateral stalk subunit P0 (*RPLP0*)	TCGACAATGGCAGCATCTAC	ATCCGTCTCCACAGACAAGG
RGS5	AGAAACCAGCCAAGACCCA	GGAGTTTGTCCAGGGAATCAC

Table 15: siRNAs for cell transfection

All siRNAs were purchased from Sigma-Aldrich (Steinheim, Germany).

siRNA	**Forward sequence (5'-3')**	**Reverse Sequence (5'-3')**	**Reference**
Firefly Luciferase GL2	Forward: CGUACGCGGAAUACUUCGA[dT][dT]		VC300A2
	Reverse: UCGAAGUAUUCCGCGUACG[dT][dT]		VC300B2
MISSION®			EHU051271

esiRNA human PDGFRB (esiRNA1)			
MISSION® esiRNA human RGS5 (esiRNA1)			EHU042281

Table 16: Cell lines

Cell line	Company	Reference
Human brain vascular pericytes (hBVP)	ScienCell Research Laboratories (Carlsbad, CA, USA)	1200
Human umbilical vein endothelial cells (HUVEC), Pooled, in EGM	Lonza (Basel, Switzerland)	CC-2519

Table 17: Animals

Animal	Company
Wild type C57BL/6JRj mice	Janvier Labs (Le Genest Saint-Isle, France)

3.2 Methods

3.2.1 Single-nucleus RNA-sequencing

This method has already been published by Vidal et al. 2019 and the data were submitted to the ArrayExpress database of the European Bioinformatics Institute (Accession number: E-MTAB-7869).[68] Three young (12 weeks) and old (18 months) male C57BL/6JRj mice were anesthetized with isoflurane and sacrificed by cervical dislocation. For nuclei isolation, the whole hearts were harvested, dissociated in liquid nitrogen with mortar and homogenized. After nuclei release by lysis, DAPI-stained high quality nuclei were sorted by fluorescence-activated cell sorting (FACS) (Aria III, BD Genomics). Single-nucleus RNA-sequencing (snRNAseq) library preparation was performed using the Chromium Single Cell 3' protocol (10x Genomics) (Figure 8). For barcode processing and single-cell gene unique molecular identifier (UMI) counting, the reads were aligned to Genome Reference Consortium Mouse Build 38 (GRCm38) by the Cell Ranger suite version 2.1.0 with standard parameters.

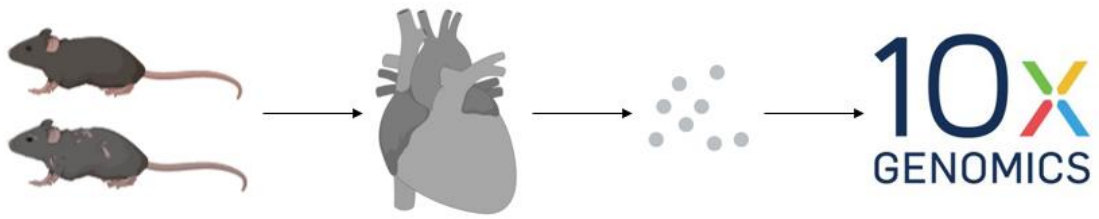

Figure 8: Schematic illustration of the snRNAseq protocol

For snRNAseq, three hearts of young and old mice were harvested and their nuclei were released by lysis. A snRNAseq library was prepared using the 10x genomics protocol.

Figure created with BioRender.com.

Results obtained from Cell Ranger were further analysed with Seurat suite version 2.2.0. Cells with less than 200 expressed genes and more than 10% mitochondrial content, as well as genes expressed in less than three nuclei were discarded, respectively. The resulting Gene-Nuclei-Expression matrix was log normalized

and scaled. Variable genes were calculated by the Seurat "FindVariableGene" function with default parameters. Canonical-correlation analysis (CCA) was performed, by the Seurat function "RunMultiCCA", to align all 6 samples and remove batch effects, which could derive from sample preparation and sequencing. t-Distributed Stochastic Neighbor Embedding (tSNE) was performed on the first 20 CCA loadings, to explore transcriptional heterogeneity and to perform dimensionality reduction for visualisation purposes. The clusters were detected on the first 20 CCA dimensions by utilising the "FindClusters" function. The Seurat function "FindAllMarkers", with default parameters (wilcoxon rank sum test), was used to identify cluster-specific genes and differentially expressed genes (DEG) between young/old. DEG were selected by selection of p-values ($P<0.05$) and false change (FC) ($FC>0.25$). Cell type assignment was performed manually based on the cluster-specific genes. Gene ontology (GO) analysis of DEG was performed using the Enrichr database.[69,70]

3.2.2 Cell culture and transfection

3.2.2.1 hBVP cell culture

hBVP cells were cultured in DMEM (high glucose, [+] L-Glutamin, [+] Sodium-Pyruvat) (Gibco Life Technologies) with 10% FBS (Gibco), 50,000 U/ml penicillin G and 50 mg/ml streptomycin (Roche). Cells were maintained maximum up to passage 10. For functional assays, cells with lower passages were preferred in order to minimize the effects of cell differentiation under culture conditions.

Cell culture flasks and dishes were always coated with a 0.2% gelatin solution in distilled water (Sigma-Aldrich) for 2 hours at 37°C. Before seeding the cells, the gelatin solution was removed from the plates and the cells were immediately seeded. For long term storage, cryopreservation was performed using culture

media containing 10% DMSO (Sigma-Aldrich) and 10% FBS (Gibco Life Technologies). This process was performed in cryogenic vials (Corning).

3.2.2.2 HUVEC cell culture

HUVEC cells were cultured in EBM (Lonza) supplemented with 10% FBS (Gibco), Amphotericin-B, ascorbic acid, bovine brain extract, endothelial growth factor, gentamycin sulfate, and hydrocortisone (EGM SingleQuots Kit, Lonza). HUVEC cells were used up to passage 4. HUVEC cells culture required no coating under these conditions.

3.2.2.3 Cell maintenance

All cells were cultured at 37°C and 5% CO_2 in a CO_2 incubator (New Brunswick™ Galaxy® 170 S, Eppendorf). Cell culture was performed using a sterile flow hood (Sterile Hood Herasafe, Hereaus). A medium change was performed every 2-3 day. Cells were splitted when reaching 80-90% confluency. To do so, the cell culture medium was aspirated (Vacuboy Hand Operator INTEGRA Biosciences) and cells were washed once with DPBS (Gibco Life Technologies). Cells were then incubated with a trypsin solution (Gibco Life Technologies, 0.25% in DPBS) for 3 minutes in the incubator. Trypsin was neutralized by adding cell culture medium. The cells were then transferred to centrifuge tube (Greiner bio-one) and centrifuged at 800 rotations per minute (rpm) for 10 minutes (Multifuge3s, Heraeus). The number of cells was determined by using the cell counter NucleoCounter (ChemoMetec), as described in the manufacturer's protocol.

3.2.2.4 hBVP siRNA transfection

Transfection of hBVPs was performed with lipofectamine for the transient silencing of gene expression by small interfering ribonucleic acid (siRNA). Hereby, Firefly Luciferase GL2 (Sigma-Aldrich) was used as siControl.

For transfection 300,000 hBVPs were seeded in 60 mm cell culture dishes (Greiner bio-one) and cultured overnight to reach 60-80% confluency. Cells were transfected with Lipofectamine™ RNAiMAX Reagent (Invitrogen).
10 µl siRNA and 5 µl lipofectamine (Invitrogen) were diluted in OPTI-MEM (Gibco Life Technologies) separately and incubated for 5 minutes. Then, the two mixes were combined and the resulting solution was incubated for 20 minutes. During this time, the cell culture medium was replaced with 2.5 ml OPTI-MEM (Gibco Life Technologies) and after the 20 minutes incubation, 515 µl of the transfection mixture was added to the cells and the dishes were incubated for 4 hours. After this time, the transfection medium was replaced with 3 ml of fresh cell culture medium and left 48 hours or 72 hours before analysis.

3.2.2.5 Viral transfection for labelling of hBVPs with GFP

Green fluorescent protein (GFP) expression by hBVPs was achieved by transfection with GFP expressing lentivirus. To do so, plasmids for viral vectors were prepared using the EndoFree Plasmid Maxi Kit (Qiagen).

Lentivirus stocks were produced in HEK293T cells. HEK293T cells were cultured in DMEM (high glucose, [+] L-Glutamin, [+] Sodium-Pyruvat) (Gibco Life Technologies) containing 10% FBS (Gibco) and 50,000 U/ml penicillin G/ 50 mg/ml streptomycin (Roche). For lentivirus production, HEK293T cells were transfected using GeneJuice® Transfection Reagent (Sigma-Aldrich). GeneJuice was diluted in OPTI-MEM according to the manufacturer's instructions. This mixture was vortexed for 3 seconds and incubated for 10 minutes. Furthermore, lentiviral expressing plasmids pMD2.G, pCMVΔR8.91, and SEW were generated like in Wagner et al. 2020.[71] In brief, 2 µg of pMD2.G, 6 µg of pCMVΔR8.91 and 8 µg of SEW were diluted in 100 µl OPTI-MEM and added to the first mixture. This new mixture was then incubated for 20 minutes. HEK293T cells were cultured with

the transfection mix for 24 hours. The day after, the medium was discarded and 20 ml of fresh HEK293T cell medium was added. After another additional 24 hours the medium was stored at 4°C and replaced with fresh 20 ml HEK293T cell medium for further 24 hours. Afterwards the virus containing supernatant 2 and 3 days after transcription were pooled. The virus was concentrated using Amicon Ultra-15, PLHK Ultracel-PL Membran, 100 kDa filter tube (Merck Millipore). The pooled supernatants were centrifuged at 1200 rpm for 5 minutes to remove cell debris. Then, the supernatant was added to a filter tube and centrifuged at 2,500 g at 4°C for 30 minutes, respectively. The 40x concentrated supernatant was aliquoted and stored at -80°C.

For viral transduction, 160,000 hBVP cells were cultured in a T25 cell culture flask (Greiner bio-one) and were transducted with a 1,5-fold virus concentration (75 µl) of the stock solution.

The cells were washed three times with DPBS and medium the next day. These washing steps were repeated two days later. After two more days, the cells were washed once with DPBS, detached, transferred to a T75 cell culture flask (Greiner bio-one), cultured and used for functional assays as described below.

3.2.3 Molecular biological methods

3.2.3.1 RNA isolation

Ribonucleic acid (RNA) was isolated using the miRNeasy Mini Kit (Qiazol) following the manufacturer's provided protocol. Summarized, cells were lysated and purified in a column system. Prior to this, samples were treated with DNase I (Qiagen) for 15 minutes. RNA was eluted in 30 µl RNase-free water (Invitrogen). RNA concentration was measured with a NanoDrop™ 2000 Spectrophotometer (Thermo Scientific).

3.2.3.2 cDNA synthesis

Complementary DNA (cDNA) synthesis was performed using M-MLV reverse transcriptase (Invitrogen). 500 ng of template RNA was used in every reaction.

In parallel, reaction controls without reverse transcriptase and with 20 µl of RNase-free water (Invitrogen) instead of RNA were prepared. The following mixtures were prepared as master mixtures. Mixture 1 was added to each sample followed by a preincubation in the GeneAmp® PCR System 9700 (Applied Biosystems) for 5 minutes at 65°C. Subsequently, mixture 2 was added to the samples and a polymerase chain reaction (PCR) cycle was performed following the protocol below (Table 18).

Table 18: Protocol for reverse transcription of RNA to cDNA

Mixture 1	1 µl	Random Hexamer Primer (Thermo Scientific)
	0.4 µl	dNTP (Applied Biosystems)
	4.6 µl	RNase-free water (Invitrogen)
Preincubation: 65°C for 5 minutes		
Mixture 2	8 µl	First strand buffer (Invitrogen)
	4 µl	DTT (Invitrogen)
	1 µl	M-MLV reverse transcriptase (Invitrogen)
	1 µl	RNase inhibitor (Applied Biosystems)
PCR cycle for cDNA synthesis: 1. 25°C 10 minutes 2. 37°C 50 minutes 3. 70°C 15 minutes 4. 4°C		

3.2.3.3 Real time quantitative PCR

Real time quantitative PCR (RT-qPCR), for the quantification of the messenger RNA (mRNA) expression, was performed using Fast SYBR Green Master Mix (Applied Biosystems) and ViiA 7 Real-Time PCR System (Applied Biosystems) in a 384 well format (Table 19). GAPDH served as endogenous control gene to normalize gene expression with the 2–ΔΔCt method.

Table 19: Mastermix approach per well for RT-qPCR

Fast SYBR Green Master Mix	5 µl
RNase-free water	1.5 µl
Primer (20 µM)	1 µl
cDNA	2.5 µl

3.2.4 Functional cellular assays

Functional experiments were conducted to investigate the role of RGS5 on various cellular functions. For this purpose the hBVP cells were transfected with siRGS5 as described above**.**

3.2.4.1 MTT assay

Cell viability and metabolic activity were measured using the MTT assay. In this test, the yellow MTT reagent is reduced to its purple insoluble product formazan in an enzymatic nicotinamide adenine dinucleotide (NADH)-dependant mitochondrial reaction (Figure 9). Thereby, the amount of measured purple product correlates with the cellular metabolic activity.

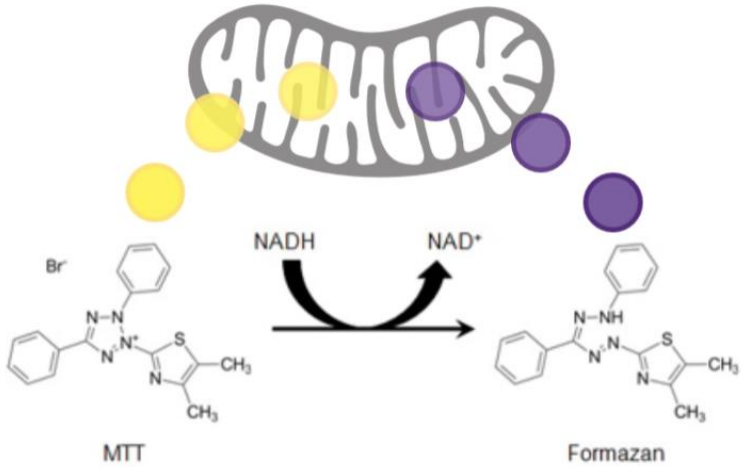

Figure 9: Schematic illustration of the enzymatic reaction of the MTT assay

The MTT assay is based on a NADH-dependent reduction of the MTT reagent taking place in the mitochondria. Thereby, MTT is transformed into its insoluble product formazan. Formazan is then released by cell lysis with DMSO and can be determined photometrical.

Figure created with BioRender.com.

To perform the MTT assay, 40,000 hBVP cells in 500 µl cell culture medium were transferred to a 24 well cell culture plate (Greiner bio-one). As controls, we used cells transfected with siControl and also untransfected hBVP cells.

After 24 hours, untransfected hBVP cells were starved for 3 hours prior to the start of the experiment with unsupplemented DMEM (Gibco Life Technologies). Meanwhile, MTT medium was prepared by diluting 10% MTT stock (Invitrogen, 5 mg/ml in DPBS) in hBVP medium. For the starving controls, an MTT mediums was prepared in unsupplemented DMEM. Cells were washed with DPBS and then 1 ml MTT medium was added to all wells. Untransfected hBVPs cultured without MTT were used as a negative control. Cells were incubated with MTT for 3 hours. Subsequently, the MTT medium was removed, the cells were washed with DPBS and incubated with 1 ml DMSO (Sigma-Aldrich) for 15 minutes on a KS 130 basic orbital shaker at 160/minute to distribute the resulting purple coloration evenly. Before incubation, the plate was carefully shaken to dissolve the emerging crystal

structures. 900 µl of the lysate was aspirated with a pipette and transferred to 1.6 ml cuvettes (Sarstedt) for spectrometric measurement in a SmartSpec Plus Spectrophotometer (Bio-Rad). To subtract the background, 900 µl DMSO were prepared as machine blank.

Permeability assay

3.2.4.1.1 Permeability assay under standard conditions

For measurement of endothelial cell permeability 24 hours after transfection, untransfected hBVP cells, siControl, and siRGS5 transfected hBVP cells were transferred with HUVECs to Thincert cell culture inserts (Greiner bio-one) (

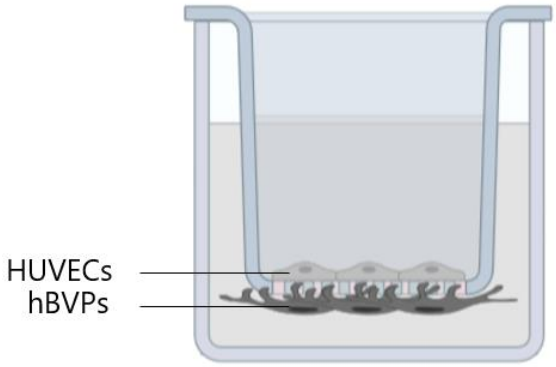

Figure 10). To do so, the inserts were first transferred to a 12 well cell culture plate (Greiner bio-one) with the membrane upwards using sterile forceps and coated for 45 minutes with 70 µl Poly-L-lysine (Sigma-Aldrich) 0.001% in distilled water per insert. The surrounding wells were filled with DPBS to prevent the membrane from drying out. During the incubation period, 450 µl DPBS was added to each well of a 24 well cell culture plate (Greiner bio-one). The inserts' inner membrane was then treated with 5 µg/cm² fibronectin (Sigma-Aldrich) diluted in 150 µl distilled water after transferring the inserts with membrane downwards onto the 24 well plate and incubated for 45 minutes. The inserts were then returned to the 12 well plate and the hBVP cells were trypsinized and centrifuged at 800 rpm for 10 minutes. 30,000 cells were diluted in 70 µl cell culture medium and added to the upper side of the membrane. Cells were incubated at room temperature for 1 hour. During this time, HUVEC cells were trypsinized and centrifuged at 800 rpm for 10 minutes. After the incubation time, the inserts were transferred again to

the 24 well plate filled with 950 µl hBVP medium. 30,000 HUVEC cells diluted in 250 µl HUVEC medium were seeded in the inner side of the membrane. The plate was incubated at 37°C overnight. The medium was changed the next day using hBVP and HUVEC medium.

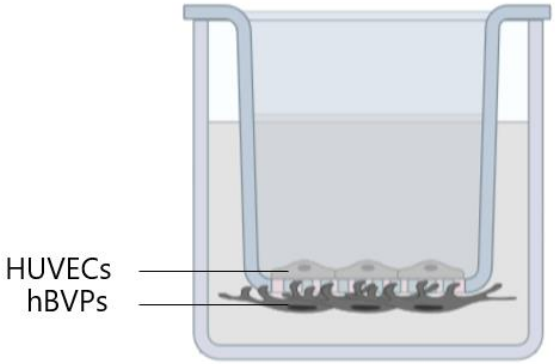

Figure 10: Experimental design of the permeability assay standard conditions

To perform the permeability assay under standard conditions, hBVP cells were transferred to the outer side that was previously coated with Poly-l-lysine, while HUVEC cells were applied to the inner membrane of cell culture inserts, coated with fibronectin.

Figure created with BioRender.com.

72 hours post transfection (p.t.), the permeability assay was performed. The medium was removed from both sides of the membrane and the cells were washed once with DPBS. 500 µl OPTI-MEM was applied to the bottom and 200 µl of FITC-dextran 1 mg/ml diluted in OPTI-MEM was added to the inserts. The cells were incubated for 1 hour. Two duplets of 100 µl were taken from the bottom of each well and transferred to a black 96 well cell culture plate (Greiner bio-one). Additional duplets of 100 µl OPTI-MEM were prepared as machine blank. The measurement was performed using the GloMax®-Multi Detection System (Promega).

3.2.4.1.2 Permeability assay with histamine treatment

Besides performing the permeability assay under standard conditions, the experiment was repeated with histamine treatment (Figure 11).

The protocol was similar to the one used under standard conditions. 80,000 HUVECs and 40,000 hBVPs were used per well in order to approach biological cell distribution. All samples were prepared as triplicates. In addition to samples with HUVECs and untransfected hBVPs, hBVPs with siControl and siRGS5 treatment, samples with HUVECs without hBVPs were prepared. These served as controls to demonstrate the effect of pericytes on endothelial permeability. Samples with HUVECs only and HUVECs with untransfected hBVPs were prepared twice to serve as negative controls without histamine treatment.

Histamine was added to the cells together with FITC-dextran in a concentration of 100 µM. Experimental measurements were conducted similar as described for the permeability under standard conditions.

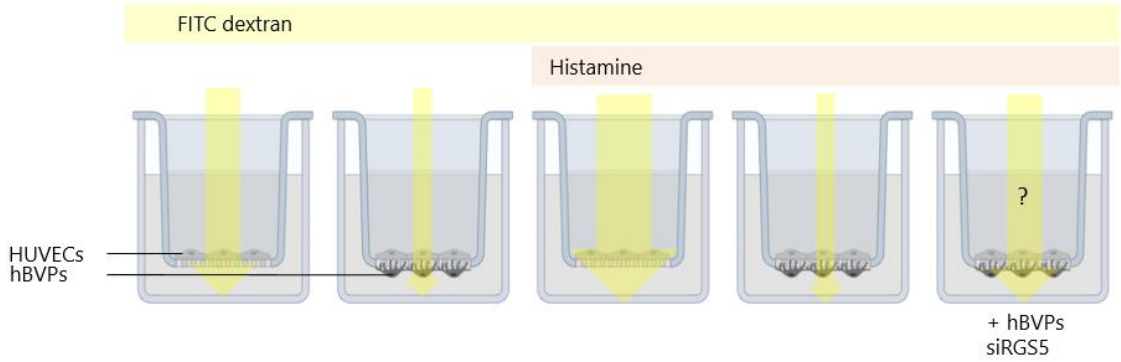

Figure 11: Experimental design of the permeability assay with histamine treatment

HUVEC and hBVP cells were prepared as described under standard conditions. Besides treatment with FITC dextran, histamine was added to test whether pericytes can compensate the increased endothelial permeability induced by histamine and whether this effect is reversed by a knockdown of *RGS5*.

Figure created with BioRender.com.

3.2.4.2 Pericyte matrix adhesion assay

The pericyte matrix adhesion assay was performed to study the ability of pericytes to adhere to a gelatin matrix or to an endothelial cell monolayer upon *RGS5* knockdown. This allowed a comparison of the adhesion under two different conditions (Figure 12).

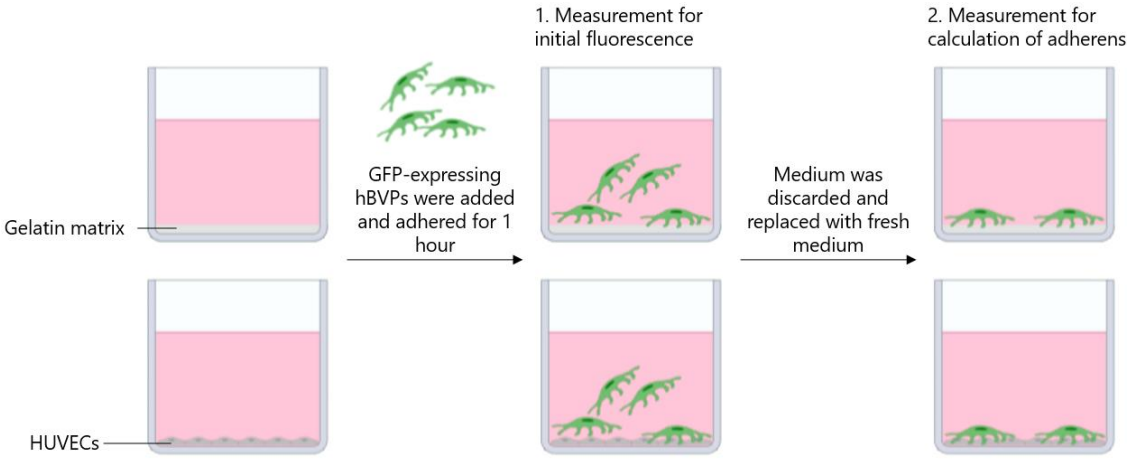

Figure 12: Experimental design of the pericyte matrix adhesion assay

GFP-expressing hBVP cells were applied to both a gelatin matrix and a HUVEC cells monolayer and allowed to attach for 1 hour. Then, the initial fluorescence intensity was measured. Medium was discarded to remove cells that had not adhered and fresh medium was added before a second fluorescence measurement.

Figure created with BioRender.com.

A sterile black 96 well cell culture plate (Greiner bio-one) was coated with gelatin 0.2% in distilled water. Three additional wells were coated, which served as blank without hBVPs. Further, HUVECs were applied to three wells per condition and three additional wells for blank and cultured for 24 hours prior to the start of the experiment.

Before starting, the plate was washed two times with 200 µl DMEM supplemented with 0.05% BSA. GFP-expressing virus transfected hBVP cells were trypsinized and

centrifuged at 800 rpm for 10 minutes 48 hours after siRNA transfection. Then 50,000 hBVP cells were seeded in the 96 well plate diluted in 100 µl DMEM supplemented with 0.05% BSA. The hBVP cells were allowed to adhere by incubating them for 1 hour at 37°C and the initial fluorescence intensity was measured photometrical for normalization using a BioTek Synergy™ HT Multi-Detection Microplate Reader (BioTek) using the Gen5™ Software (BioTek). Then, the cell culture medium was discarded to remove the hBVPs that were not attached to the gelatin, nor the HUVEC layer and 100 µl of pre-warmed 0.05% BSA in DMEM were added. The fluorescence intensity of the adhering hBVPs was measured again after this washing step by performing a second photometrical measurement. The background was subtracted by samples containing no GFP-expressing hBVPs separately for each condition. For quantification, the first measurement was compared to the second to determine the relative decrease in the amount of hBVPs.

3.2.4.3 Endothelial tube adhesion assay

The endothelial tube adhesion assay (Figure 13) was performed in a 3D Matrigel Matrix (Gibco Life Technologies), which allowed the formation of tubes by endothelial cells. To allow imaging, the experiment was performed using viral transfected GFP-expressing hBVPs, which were subsequently transfected with siRNA as described above. HUVEC cells were stained in red with human DiI-Ac-LDL (Invitrogen) the day before the start of the assay. 400,000 HUVEC cells were seeded in a 60 mm cell culture dish (Greiner bio-one). After 24 hours of incubation, the medium was removed and HUVEC cell culture medium with 10 µg/ml DiI-Ac-LDL was added to the cells and incubated overnight at 37°C.

For experimental preparation, the gel was placed on ice at 4°C for liquification the day before the start of the experiment. 1000 µl pipette tips and a 48-well cell culture plate (Greiner bio-one) were cooled down at -20°C overnight. Afterwards,

the Matrigel was always kept on ice to prevent premature polymerization at room temperature.

One layer of 150 µl of the thawed gel was added evenly to the bottom of the pre-cooled 48 well plate and incubated at 37°C for 30 minutes. During this incubation, the Dil-Ac-LDL stained HUVEC cells were trypsinized and centrifuged at 800 rpm for 10 minutes. 100,000 cells diluted in 500 µl cell culture medium were then seeded on top of the gel of each well and incubated for 3 hours at 37°C. Then, GFP-expressing siControl and siRGS5 transfected hBVP cells were trypsinized, centrifuged at 800 rpm for 10 minutes. 10,000 cells were seeded on top of the HUVEC cells after tube formation and incubated for another 3 hours. Afterwards, the medium was removed and another layer of 150 µl Matrigel was added and incubated for 30 minutes at 37°C. Then 500 µl cell culture medium consisting of hBVPs medium and HUVEC medium in equal parts were added to the gel. After overnight incubation, the cells were fixed in ROTI® Histofix 4% (Carl Roth) at 4°C in the Matrigel for 30 minutes. Images were taken 72 hours after transfection with a Leica SP8 confocal microscope.

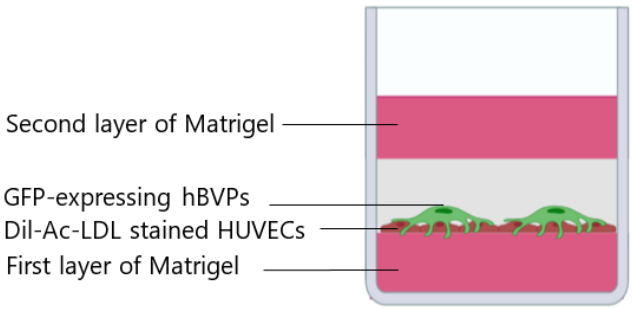

Figure 13: Experimental design of the endothelial tube adhesion assay

Red Dil-Ac-LDL-stained HUVEC cells were applied to a layer of Matrigel and allowed to form tubes before GFP-expressing hBVPs were added. A second layer of Matrigel was added and the cells incubated overnight. Fixation and microscopic analysis was performed the following day.

Figure created with BioRender.com.

Image analysis was performed by using Volocity (Quorum Technologies), measuring nine representative images of every heart. Thereby, the number of detaching hBVPs was captured. For this purpose, the total number of hBVPs per image was counted and subsequently the number of hBVPs with the formation of filopodia-like extensions was determined. The number of hBVPs that were completely spherical was not included in the quantification. In order to compare the number of detached hBVPs with the number of HUVECs, the area of the DiI-Ac-LDL stained HUVECs was measured. The ratio of detached hBVPs to the measured area was then calculated.

3.2.5 Cryo-section immunostaining

3.2.5.1 Tissue processing

Hearts from young (12 weeks) and old (18 months) wild type C57BL/6JRj mice were harvested and dissected in cold PBS. Fixation was performed in ROTI® Histofix 4% (Carl Roth) at 4°C overnight. Subsequent overnight washing steps with DPBS in ascending sucrose (Sigma-Aldrich) concentrations of 10%, 20% and 30% were performed for cryo-sectioning to achieve cryo-protection followed by embedding in embedding solution (15% sucrose, 8% gelatin Gelatin from porcine skin (Sigma-Aldrich) and 1% PVP (Sigma-Aldrich) in DBPS) until solidification. Samples were frozen at -80°C and sectioned with a thickness of 50 µm using the Leica CM3050 S cryostat. Then, samples were dried on microscope slides (SuperFrost Plus™ Adhesion slides, Thermo Scientific) at room temperature overnight and stored at -20°C until use.[72]

3.2.5.2 Rgs5 *immunostaining*

Cryo-sections from young and old mouse hearts were thawed at room temperature and rehydrated in a coplin jar in DPBS three times for 5 minutes. Antigen retrieval was performed in a 10 nM tri-sodium citrate dihydrate. (Carl

Roth). This was pre boiled in a 2 l plastic beaker in a microwave. Slides were added and boiled for 10 minutes and let cool down on ice for 30 minutes.

This procedure was followed by four washing steps with distilled water and one washing step with DPBS. To quench endogenous peroxidases, the slides were incubated for 40 minutes in 3% hydrogen peroxide (Carl Roth) diluted in 100% methanol (Fisher Chemical). The slides were washed again three times for 5 minutes with DPBS. Tissue was permeabilized with 0.3% triton X-100 on DPBS three times for 10 minutes. The blocking solution (Table 20) was freshly prepared and the slides were blocked 1 hour at room temperature in a humified chamber.

Table 20: Staining solutions

Permeabilisation solution	0.3% triton X-100 (Sigma-Aldrich)
	in DPBS
Blocking solution	3% BSA (Sigma-Aldrich)
	0.1% triton X-100
	2% $MgCl_2$ (Carl Roth)
	5% Normal Donkey Serum (Jackson ImmunoResearch Laboratories)
	in DPBS

Primary antibodies were added in the listed concentrations (Table 21) in 150 µl blocking solution and incubated overnight at 4°C in a humified chamber covered by parafilm (Sigma-Aldrich).

Table 21: Primary antibody concentrations

Rgs5 Polyclonal Antibody (Invitrogen)	1:100
Fluorescein labeled Griffonia (Bandeiraea) Simplicifolia Lectin I (Vector Laboratories)	1:25

Prior to secondary antibody incubation, slides were washed in DPBS for 5 minutes and once with triton 0.3% in DPBS. Secondary antibodies were added at the listed concentrations (Table 22) in 150 µl 5% BSA in DPBS per slide and incubated for 1 hour at room temperature in a humified chamber covered by parafilm.

Table 22: Secondary antibody concentrations

Polyclonal Goat Anti-Rabbit Immunoglobulins/Biotinylated (Dako)	1:100
Hoechst 33342 Staining Dye Solution (Abcam)	1:1,000

At the same time, the VECTASTAIN® Elite® ABC HRP Kit (Vector Laboratories) was prepared according to manufactures instructions and incubated for 1 hour at room temperature. After the incubation period, the slides were washed two times in DPBS for 5 minutes with a subsequent quick wash with 0.3% triton in DPBS. Then 200 µl of the ABC solution was added and incubated for 1 hour covered by parafilm in a humified chamber. This was followed by a repetition of the previous washing steps. TSA Cyanine 3 Tyramide Reagent (Perkin Elmer) was prepared 1:100 in the included solution and added to the slides for 5 minutes covered with parafilm. The slides were washed again two times with DPBS for 5 minutes and were mounted with Fluorescence Mounting Medium (Dako) before adding the coverslips (Thermo Scientific Menzel). After 30 minutes incubation at room temperature, the slides were stored at 4°C. Immunostainings were imaged in a Leica SP8 confocal inverted microscope.

3.2.6 Statistical analysis

Statistical analysis was performed using the Prism8 Software (Graphpad). All data are presented as means. Error bars show standard errow of the mean (SEM). A normality test was performed to check for normal (Gaussian) distribution. Normally distributed groups were then analysed by using an unpaired t test. Not

normal distributed groups were tested using the Mann-Whitney test. Analysis of more than two groups was performed by application of an ordinary-one-way ANOVA test.

4 Results

4.1 Regulation of pericyte genes in the aging heart

4.1.1 Single-nucleus RNA-sequencing shows that the expression pattern in pericytes is changed in the aged heart

To study the cellular heterogeneity in the heart during aging, snRNAseq was performed on three young (12 weeks) and old (18 months) male mouse hearts. Hereby 14,827 nuclei from cells from young hearts and 12,981 nuclei from cells from old hearts were analyzed. Subsequent tSNE was used for visualization of the distribution of young (blue) and old (red) nuclei (Figure 14A). In total 17 clusters were defined through the selection of specific cellular markers. These markers identified 7 cell types in the clusters, including cardiomyocytes (cluster 0, 2, 11, 16), fibroblasts (cluster 1, 5, 12), endothelial cells (cluster 3, 4, 10), immune cells (cluster 6, 7, 13), pericytes (cluster 8, 15), epicardial cells (cluster 9) and granulocytes (cluster 14) (Figure 14B, C). The raw data set has been already published in Vidal et al 2019.[68] In this work, we focused on the detailed analysis of cluster 8 and 15, the two clusters identified as pericytes.

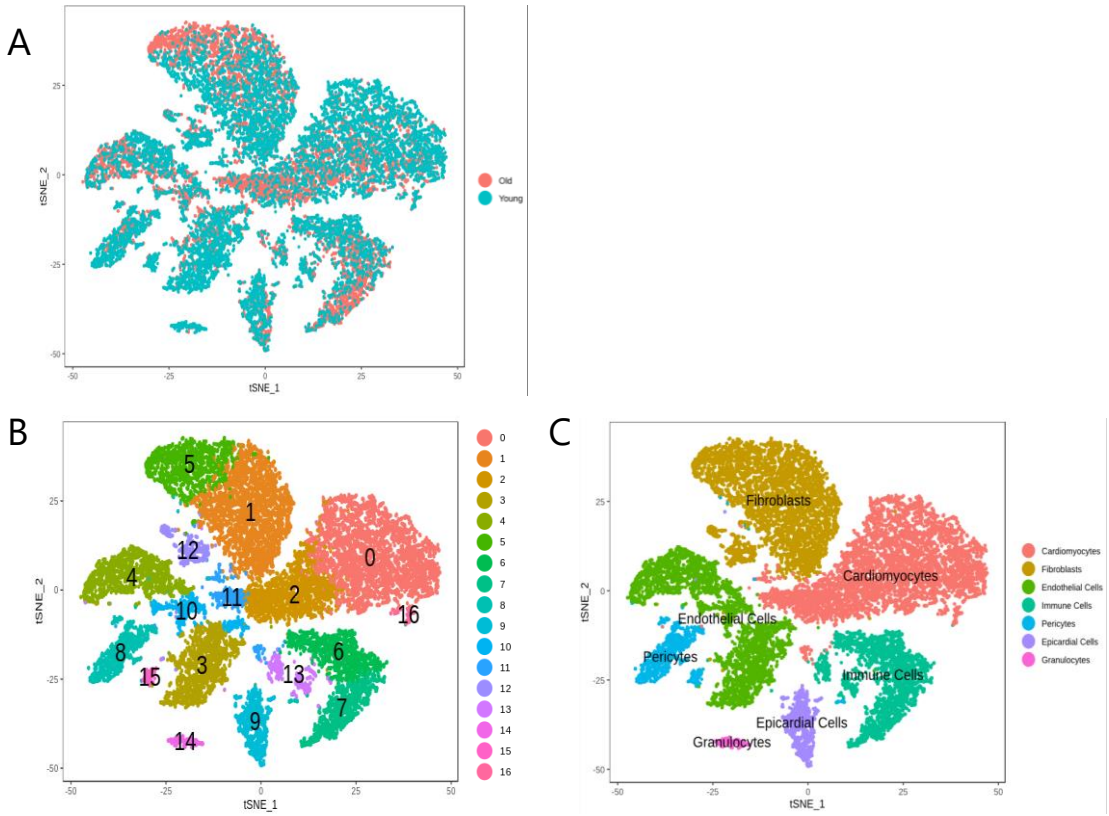

Figure 14: Cellular heterogeneity in the aging heart

(A) tSNE plots representing distribution of all cells of three young (12 weeks), shown in blue, and old (18 month), shown in red, mouse hearts. (B) 17 different clusters could be defined that were assigned to (C) seven cell types through selection of specific cellular markers.

4.1.2 *Rgs5* expression is downregulated in pericytes in the aging heart

To analyse the pericyte-specific regulated genes, all pericytes were selected by expression of *Pdgfrb* and chondroitin sulfate proteoglycan 4 (*Cspg4)*, also known as *Ng2,* which are known cellular markers for pericytes (Figure 15A, B). It is noteworthy, that clustering only the pericytes did not lead to clusters that are exclusively populated by young and old pericytes (Figure 15C).

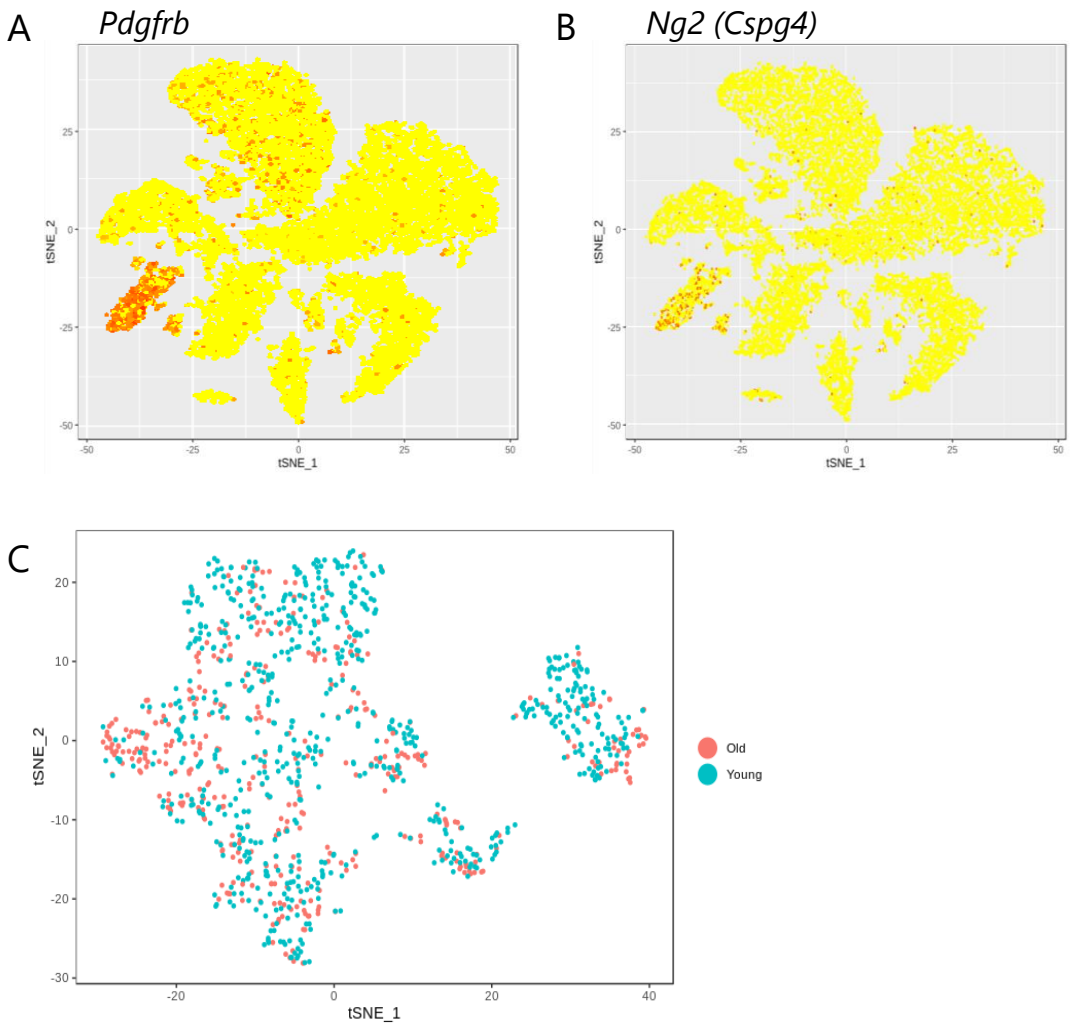

Figure 15: Pericyte population in the heart

tSNE plots showing pericyte clusters through selection of (A) *Pdgfrb* and (B) *Ng2* as pericyte-specific markers. (C) distribution of young (blue) and old (red) nuclei in pericyte clusters.

We then analyzed the DEG in young and old pericytes. We identified a total of 336 DEG, 244 downregulated and 92 upregulated in the old pericytes. Among the top 20 upregulated and downregulated we found some genes like Chemokine C-C motif ligand 8 (*Ccl8*), Signal transducer and activator of transcription 3 (*Stat3*) and Vitronectin (*Vtn*) (Figure 16). Ccl8 belongs to the family of CC-chemokines and is relevant for leukocyte chemotaxis and different inflammatory diseases.[73] Stat3, a member of the Stat protein family, also participates in the immune response. It is activated by a variety of molecules, including cytokines and growth

factors, and plays a role in different physiological processes.[74] Vtn is a glycoprotein of the extracellular matrix and regulates cell attachment, proliferation, differentiation and migration through binding to integrin receptors.[75] In pericytes, these genes are relevant for the modulation of the cerebral immune response, the regulation of angiogenesis in cerebral ischemia and for developmental processes in neurogenesis.[75–77]

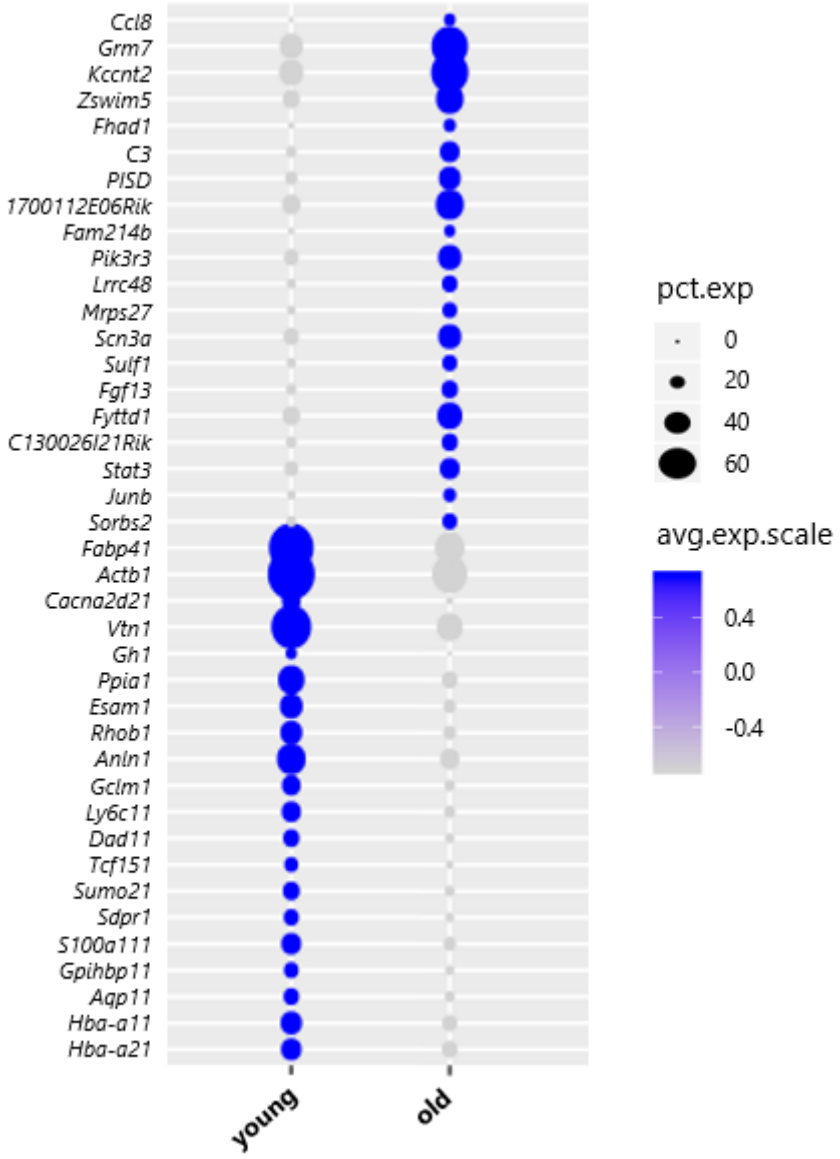

Figure 16: Differentially expressed genes in young and old pericytes

Dot plot showing the top 20 DEG regulated in young and old pericytes as percentage of expressing cells (pct.exp) and average scaled expression (avg.exp.scale).

Among the regulated genes, *Rgs5* was strongly downregulated in pericytes from the old hearts. The different expression of *Rgs5* in pericytes of young and old hearts was highly significant using the Wilcoxon rank sum test (P=1.13E-12) (Figure 17A). For this reason, we selected *Rgs5* to further analyse the molecular mechanisms that control pericyte aging in the heart. To do so, we analysed the the *Rgs5* expression in the heart (Figure 17B). Although *Rgs5* was widely expressed throughout other cell populations, the highest expression was linked to the pericyte clusters.

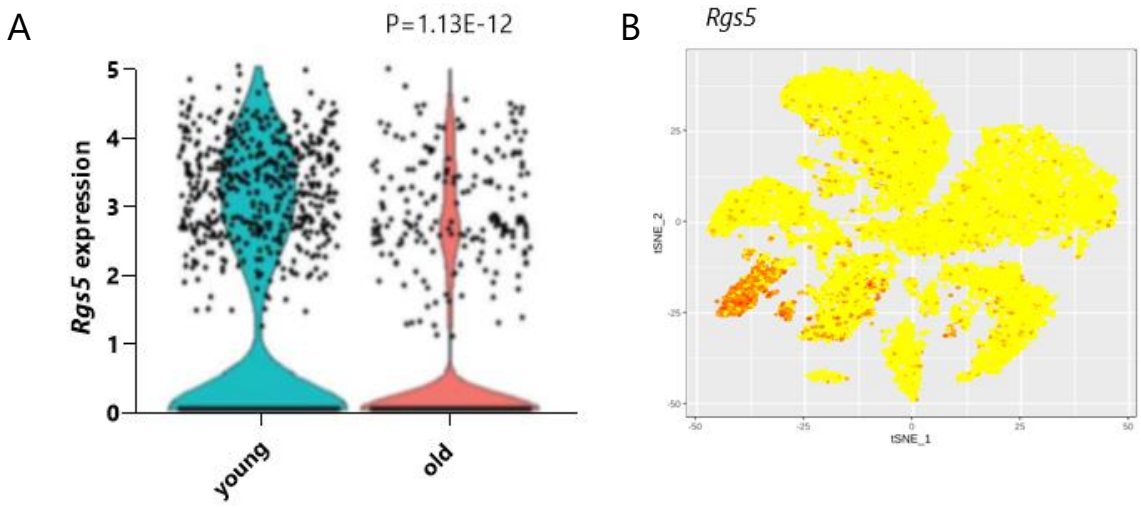

Figure 17: *Rgs5* in downregulated in the aging heart

(A) Violin plots visualising the distribution of log2 fold change of *Rgs5* expression in nuclei from pericytes of young (blue) and old (red) hearts. Statistical analysis was performed using the Wilcoxon rank sum test. (B) tSNE plot showing the expression of *Rgs5* in the heart. The expression of *Rgs5* corresponds to the pericyte clusters.

4.1.3 GO analysis of DEG in pericytes revealed a downregulation in genes related to cellular adhesion

To gain further knowledge in the function of the DEG in aged pericytes, we performed a GO analysis of DEG.

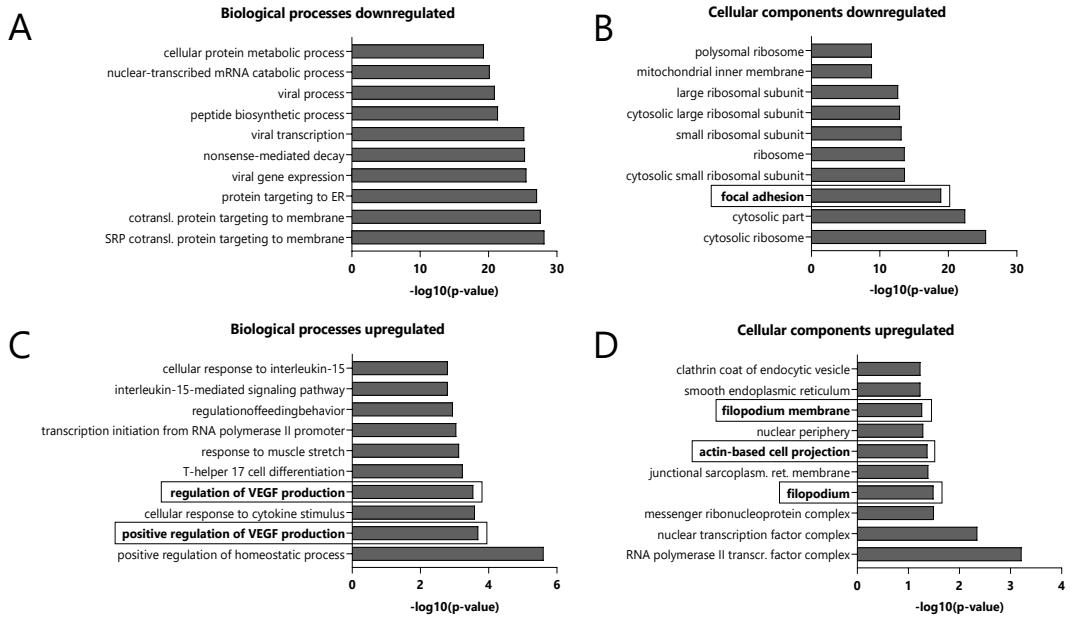

Figure 18: GO analysis of DEG in young and old pericytes suggests a loss of adhesion and increased motility of old pericytes

Representation of the ten most significant functional categories in each group revealed by GO analysis using the Enrichr data base. Graphs represent negative logarithmic p-value. Biological processes (A, C) and cellular components (B, D) of down- (A, B) and upregulated (C, D) genes.

The analysis of genes downregulated in the aged pericytes showed a downregulation of genes related to cellular components associated with focal adhesion points (Figure 18A, B). This group of genes was assigned to a variety of ribosomal proteins and actin subtypes, as well as proteins involved in the mitogen-activated protein kinase (MAPK) signaling pathway (Table 23).

Furthermore, the upregulated genes in old pericytes were related to biological processes regulating the vascular endothelial growth factor (VEGF) production. Other genes upregulated in old pericytes were associated with filopodia, filopodia membrane and actin-based projection (Figure 18C, D). The upregulation of these genes may be related to processes like migration and motility in an angiogenesis related fashion. In contrast to the downregulated genes, the involved upregulated processes comprised only a small number of genes, including dystrophin (*Dmd*), fibroblast growth factor 13 (*Fgf13*), complement component 3 (*C3*), retinoid acid

receptor-related orphan receptor alpha (*Rora*) and sulfatase 1 (*Sulf1*) (Table 23). Dmd is a cytoplasmic protein of the musculature that connects the cell membrane to the extracellular matric. An absence or dysfunction of Dmd leads to the development of muscular dystrophies.[78] Fgf13 is a microtubule-stabilizing protein, relevant for neuronal migration,[79] as well as for tumor metastasis.[80] C3 is part of the complement cascade of the coagulation, also functioning as a pro-inflammatory and immunoregulatory protein.[81] Rora is a nuclear receptor acting as a key regulator of different physiology processes such as circadian rhythm, angiogenesis, bone morphologies and the development of the retina. Rora is also known as a part of signaling pathways that are involved in inflammation and immune response.[82] Finally, sulf1 is involved in the conversion of heparan sulfate, a protein of the extracellular matrix, by removing sulfate groups. In addition, sulf1 acts as a regulator of many signaling pathways and is probably involved in the brain development.[83] Changes in the extracellular matrix and in the cytoskeleton of cardiac pericytes could explain the phenotype observed in the aged mural cells.

Table 23: Regulated genes from GO categories

	GO analysis	**Categories**	**Genes**
downregulated	cellular components	focal adhesion	*Cd81, Rplp0, HsPb1, Rpl8, Actb, Rpl6, Rpl7, Actg1, Rps15, Rps4x, Rps18, Tspan9, Cfl1, Rps3, Rps11, Rpl18, B2m, Pdia3, Hspa9, Hspa8, Rps9, Map2k1, Rps7, Rpl23, Anxa5,*

			Rhoa, Rhob, Marcks, Actc1, Rps29, Pfn1, Ppib, Ppia
upregulated	cellular components	filopodium membrane	*Dmd*
		actin-based projection	*Dmd, Fgf13*
		filopodium	*Dmd, Fgf13*
	biological processes	positive regulation of VEGF production	*C3, Rora, Sulf1*

We validated our GO observations using PANTHER, another GO database.[84] This confirmed the deregulation of adhesion, cellular organization and locomotion (Figure 19). In addition to the genes linked to focal adhesion by Enrichr, PANTHER returned Nexilin (*Nexn)* as another gene relevant for biological adhesion in upregulated genes in aging. *Nexn,* also known as F-actin binding protein, is important for cell migration and adhesion.[85,86] It has been previously described to be involved in the modulation of vSMC phenotype and differentiation,[87] as well as in the development of dilated cardiomyopathy and coronary artery disease (CAD).[88,89]

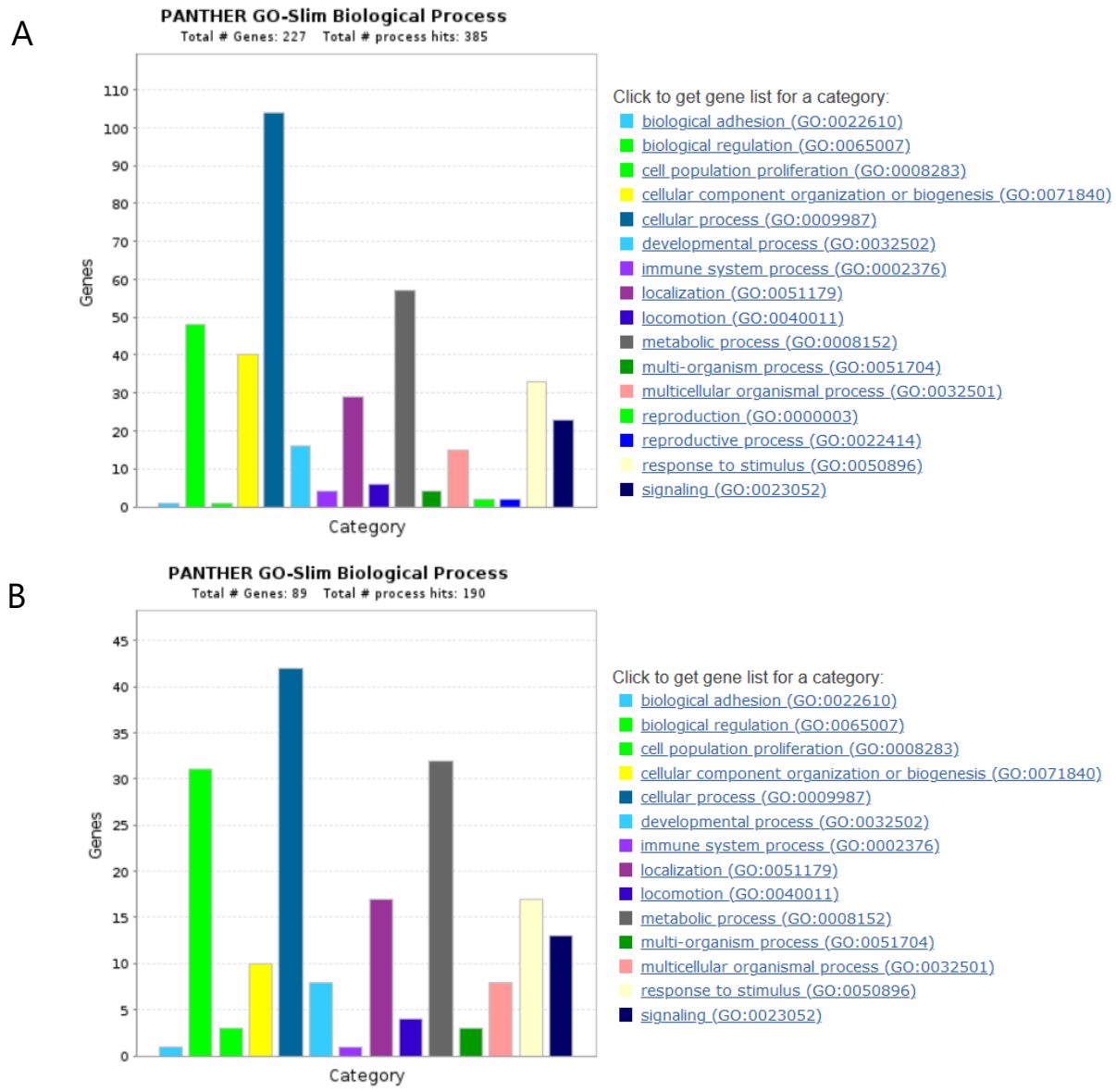

Figure 19: Validation of GO analysis results

Gene ontology analysis using the PANTHER Classification System. Graphs show the number of genes regulated in relevant categories of biological processes (A) downregulated and (B) upregulated in aging pericytes.

4.1.4 Rgs5 is downregulated in the aged heart

We furthermore validated the downregulation of Rgs5 *in vivo*. To do so, we performed immunostainings in young (12 weeks) and old (18 months) wild type hearts of male C57BL/6JRj mice (Figure 20A). We then quantified the area covered by Rgs5 immunosignal and normalized with the area covered by Lectin

immunosignal, which specifically binds to the surface of endothelial cells.[90] This revealed a significant reduction of Rgs5 expression in the old heart (Figure 20B).

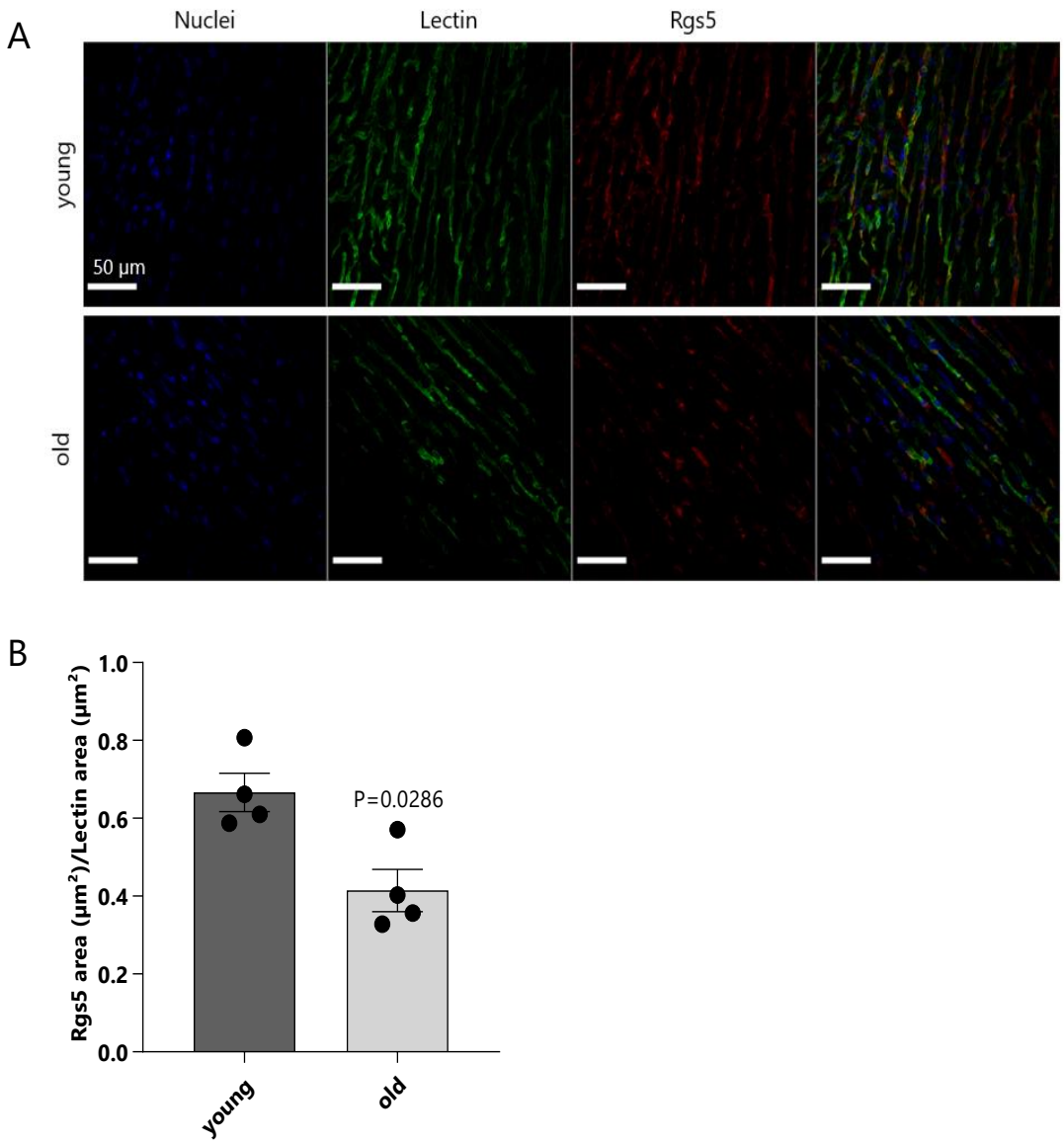

Figure 20: Rgs5 expression is reduced in old hearts

(A) Immunohistochemistry on sections of young and old hearts. Hearts were labeled with Fluorescein labeled Griffonia (Bandeiraea) Simplicifolia Lectin I (green) and Rgs5 (red). Nuclei were stained with Hoechst 33342 (blue). (B) Quantification of measured Rgs5 area in µm² compared to Lectin area in µm² in young and old hearts. Data represented as mean ± SEM. per group (N=4). P-value was calculated by nonparametric two tailed Mann-Whitney test.

4.2 Regulation of pericyte function by *RGS5*

To further study the effects of a reduced *RGS5* expression in pericytes during aging we performed functional analyses *in vitro* using hBVPs, an established pericyte cell line. Our hypothesis is that the knockdown of *RGS5* using siRNA might induce a premature aging effect on the pericytes.

We tested the efficiency of the *RGS5* knockdown using different concentrations of siRNA and different time points after transfection. To reduce possible cytotoxic effects, we titrated the concentration of 67 nM suggested by the manufacturer. Our results indicate that a siRNA concentration of 67 nM is required for the efficient knockdown of *RGS5* (Figure 21A). Moreover, 24 hours are sufficient to efficiently and significantly knockdown *RGS5* expression (Figure 21B). Taking into account these results, we adopted 67 nM siRNA concentration and 48 hours after transfection for our functional assays.

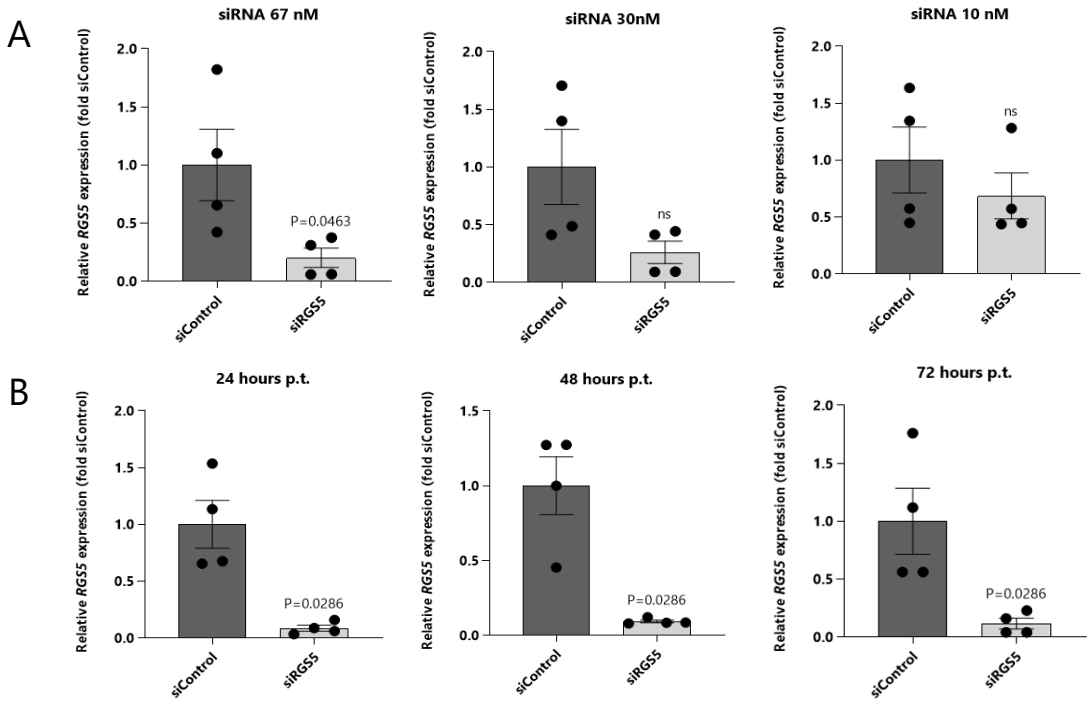

Figure 21: Knockdown efficiency of siRGS5 in hBVP cells

Knockdown efficiency of *RGS5* in hBVPs after treatment with (A) siRNA concentration used for 24 hours (N=4) and (B) time dependency after treatment with siRNA with concentration of 67 nM

(N=4). Data shown as mean ± SEM. Statistical analysis was performed using the nonparametric two tailed Mann-Whitney test.

4.2.1 *RGS5* knockdown does not affect pericyte viability nor metabolic activity

In order to determine whether *RGS5* knockdown leads to a reduced viability or a change in the metabolic state of the pericytes, we performed a MTT assay in hBVPs. We could not detect any difference in the metabolism of MTT upon *RGS5* knockdown (Figure 22A). We furthermore went on to serum starve the cells, but we could still not detect any difference (Figure 22B).

It was also investigated whether starvation of *RGS5* knockdown cells induces an additional effect compared to standard conditions. Again, no reduction of cellular viability was observed.

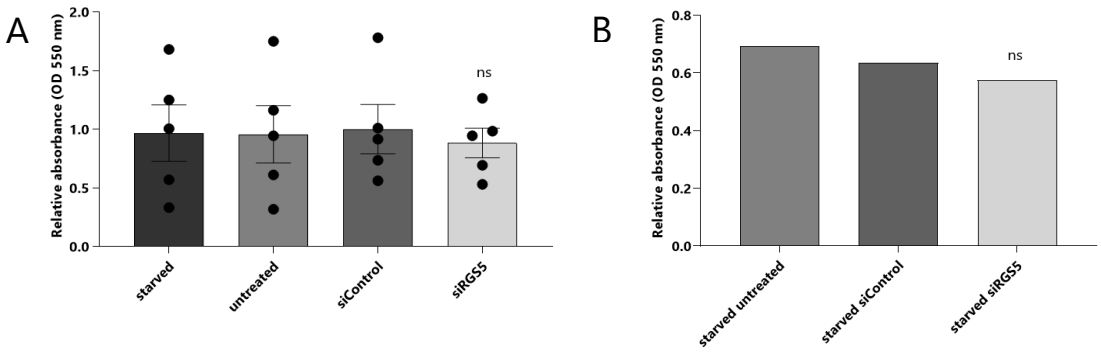

Figure 22: *RGS5* knockdown does not reduce cellular viability *in vitro*

(A) Data shown as mean ± SEM of independent experiments performed 48 hours p.t. with a MTT incubation of 3 hours (N=5), measured at an optic density (OD) of 550 nm. (B) Data of one representative experiment evaluating the effect of 3 hours starvation before MTT incubation (N=1). Values were calculated using one-way ANOVA test. Not significant (ns).

4.2.2 Endothelial permeability is not affected upon pericyte *RGS5* knockdown

One of the functions most studied on pericytes, albeit in brain pericytes, is their maintaining BBB.[91] To evaluate if *RGS5* knockdown in hBVPs affects endothelial cell permeability, we established a pericyte-endothelial cell co-culture assay using Thincert cell culture inserts with a pore diameter of 1 µm. We applied HUVEC cells to the inner face and hBVPs to the outer face of the membrane, as described above. 72 hours after knockdown of *RGS5* the flow rate of FITC dextran through the membrane was measured photometrically. The amount of FITC dextran that flows through the membrane is directly correlated to the permeability of the endothelial cell monolayer that has grown in it. We compared siRGS5 pericytes to both, untransfected hBVPs and siControl transfected pericytes. Endothelial permeability was not significantly changed upon pericyte transfection with siRGS5 (Figure 23).

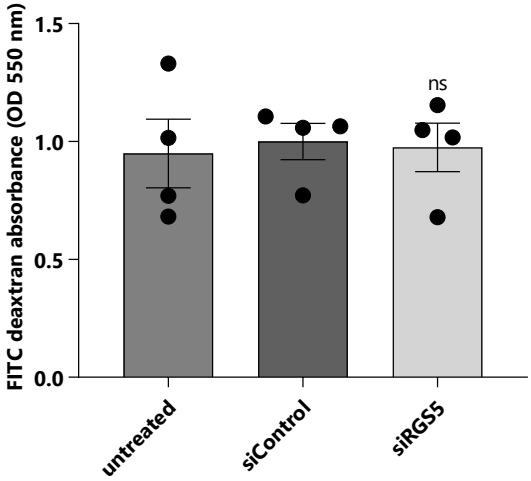

Figure 23: *RGS5* knockdown in hBVPs does not affect endothelial permeability

Data shown as mean ± SEM of independent experiments (N=4). FITC dextran absorbance was measured 1 hour after application at an OD of 550 nm. Statistical analysis was performed using ordinary one-way ANOVA test.

We decided to challenge the setting. To do so, we repeated the permeability assay treating the cells with histamine. Histamine is a vasoactive substance that has

been already described as an inducer of endothelial permeability by disruption of focal adhesion contacts.[92]

We added histamine at the same time as FITC dextran and continue its flow trough. The treatment with histamine led as expected to an increased endothelial permeability and this effect could be compensated by the coculture of endothelial cells with untransfected hBVPs. Still, we could not observe any difference between control and siRGS5 pericytes (Figure 24).

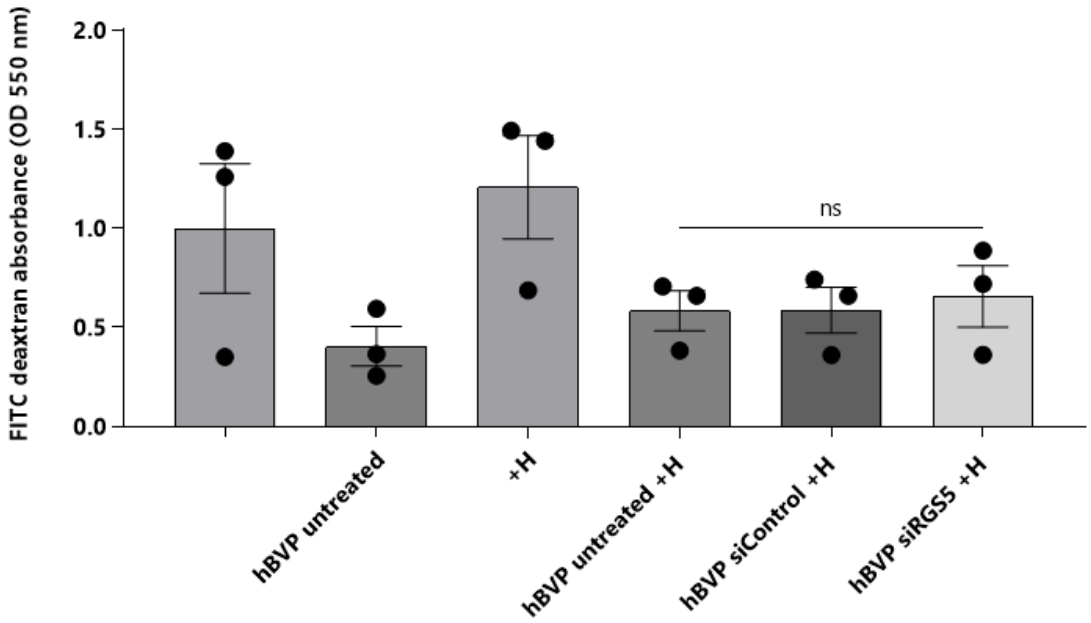

Figure 24: *RGS5* is dispensable for permeability regulation in hBVPs

Data shown as mean ± SEM of independent experiments (N=3). FITC dextran absorbance was measured 1 hour after application at an OD of 550 nm. All samples contained HUVECs. Different application of hBVPs and treatment with histamine (+H) was performed as described in the labeling. Statistical analysis was performed using ordinary one-way ANOVA test.

4.2.3 RGS5 knockdown reduces adhesion of pericytes *in vitro*

To investigate the adhesion behaviour of hBVPs upon *RGS5* knockdown, we performed a pericyte-matrix adhesion assay. In short, we seeded control and

RGS5 transfected hBVPs into plates coated with gelatin or on top of a HUVEC monolayer and measured photometrical the cellular adhesion after a series of washes. It is noteworthy that upon *RGS5* knockdown hBVPs present a reduction of cellular adhesion when compared to control counterparts (Figure 25).

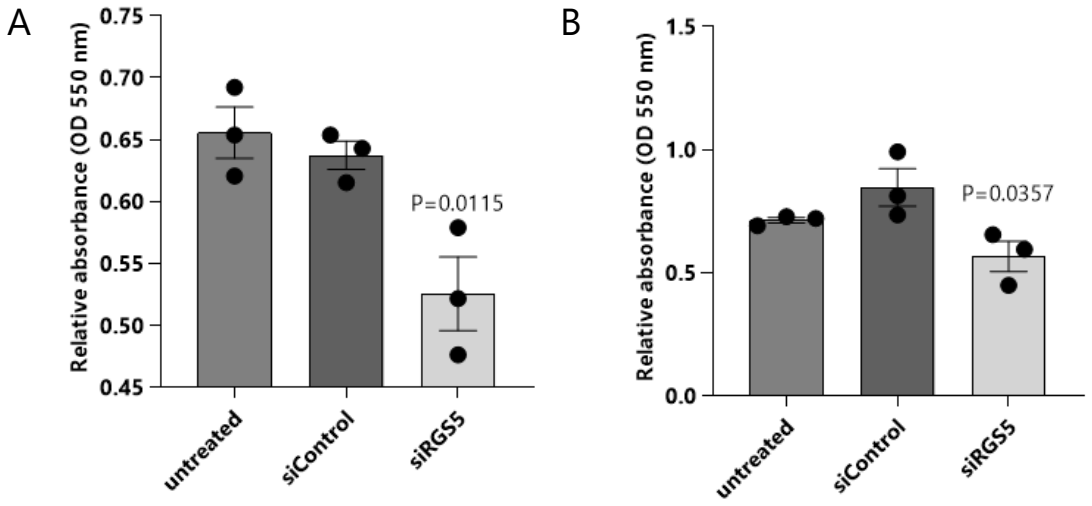

Figure 25: *RGS5* knockdown reduces pericyte adhesion to a gelatin matrix and to endothelial cells

Data shown as mean ± SEM (N=3) performed under two different conditions using (A) coating with gelatin and (B) a monolayer of HUVECs. FITC dextran absorbance was measured at an OD of 550 nm. P-value was calculated using ordinary one-way ANOVA test.

To further study the effect of *RGS5* knockdown to pericyte adhesion, we performed a co-culture of GFP-labeled hBVPs together with Dil-Ac-LDL labelled HUVECs in Matrigel. The labelled cells would allow us to take microscopy images and analyze the relationship between the two cell types. HUVEC cells were allowed to form tubes before pericytes were applied simulating a vascular capillary bed.

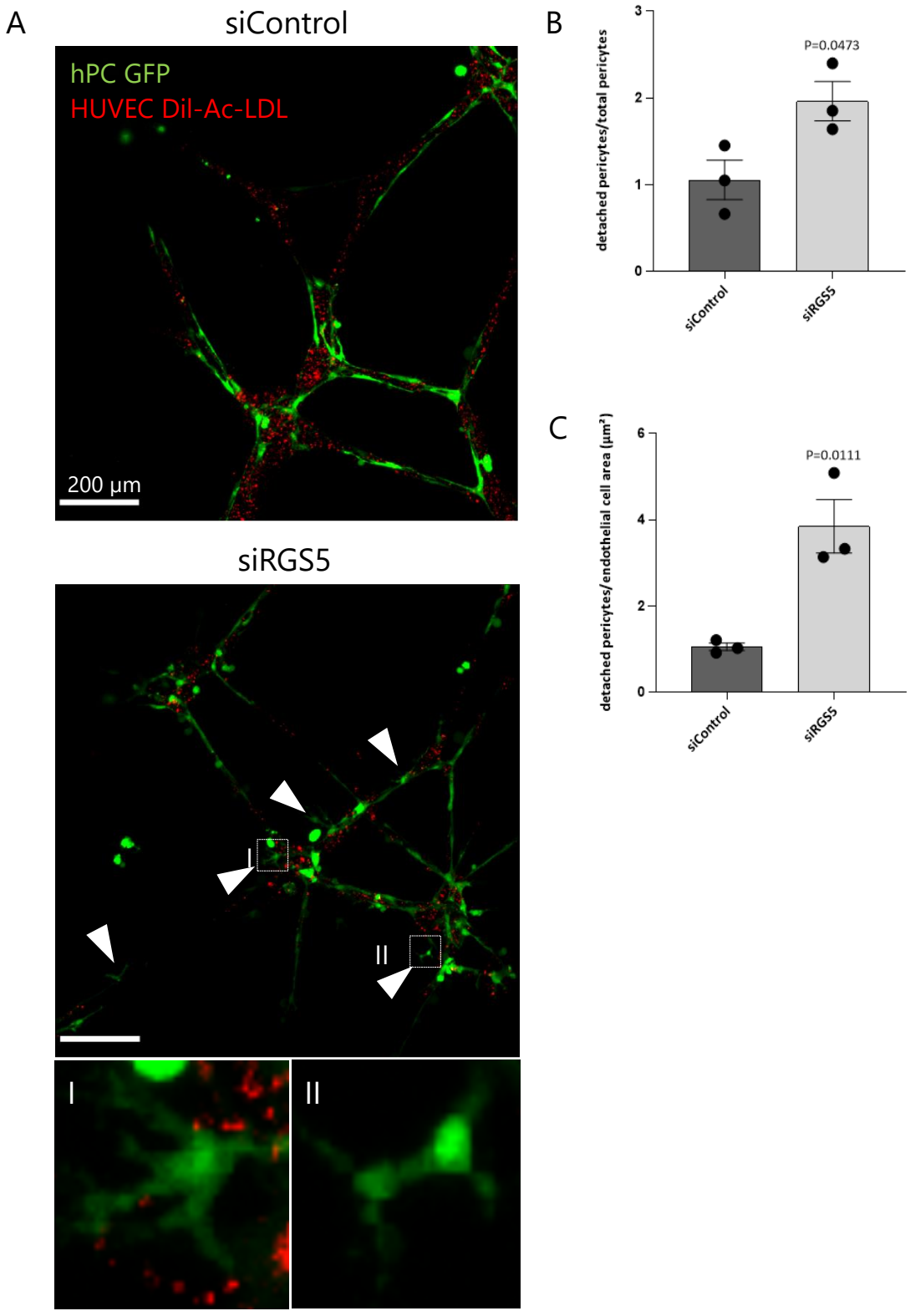

Figure 26: hBVPs detach from endothelial cells and develop filopodia-like structures after knockdown of *RGS5 in vitro*

(A) Representative confocal images of co-culture Matrigel assay showing siControl and *RGS5* knockdown GFP-expressing hBVPs (green) and DiI-Ac-LDL uptake in HUVECs (red). White arrows

point out detaching pericytes. White squares label two morphologic stages of detaching hBVPs: hBVPs with remaining contact to HUVECs under formation of filopodia (I) and hBVPs completely detached from HUVECs (II). (B-C) Quantification was performed by evaluation of 5-10 images per well of triplicates of independent experiments (N=3). Detached pericytes were counted and compared to the number of total pericytes per image (B) and the area of DiI-Ac-LDL HUVECs (C) using the Volocity Software. Data shown as mean ± SEM. For statistical analysis an unpaired two-tailed t-test was performed after testing for normal distribution.

RGS5 knockdown induced morphological changes in the hBVPs. The hBVPs detached from the endothelial tubes and formed increased cytoplasmic extensions that resemble filopodia (Figure 26A). In order to quantify the effect on cellular adhesion, we quantified the number of detached hBVPs. This evaluation with comparison of the detached pericytes to the total number showed a significant (P=0.0473) increase of detached pericytes in the *RGS5* knockdown samples (Figure 26B).

Consistent with the previous results, a significant increase (P=0.0111) of the detaching hBVPs to the endothelial cell area could be observed (Figure 26C).

4.3 Effect of *RGS5* knockdown on pericyte identity

To explain the phenomenon of reduced adhesion at lower *RGS5* expression, investigations were conducted to determine whether pericytes dedifferentiate with age or under knockdown of *RGS5*.

4.3.1 GO analysis of DEG in pericytes indicates upregulation of fibroblast-associated genes in aging

Our previous GO analysis of the DEG in the aged pericytes revealed that in old pericytes, genes that are characteristic of fibroblast were upregulated like forty-two-three domain containing 1 (*Fyttd1*), phospholipase C like 1 (*Plcl1*), collagen type V alpha 2 chain (*Col5a2*) and TEA domain transcription factor 1 (*Tead1*) (Figure 27). Fyttd1, also known as UAP56-Interacting Factor (UIF), is a mRNA

export adapter protein for the transport of mRNA to the nuclear pore.[93] COL5A2 encodes an alpha chain of fibrillar collagen. Mutations of COL5A2 are responsible for the Ehlers-Danlos syndrome. There may also be a link between COL5A2 and the repair mechanisms of the heart after an infarction in association with ischemic cardiovascular disease.[94] TEAD1, also known as transcriptional enhancer factor 1 (TEF1), is a transcription factor involved in the positive regulation of the gene expression in muscles and the placenta.[95]

Some of these genes have already been described as relevant in fibroblast biology. For example, collagen subtypes, including COL5A2, are widely expressed in cardiac fibroblasts.[96] Further, the family of TEAD proteins is involved as transcription factors in the downstream signaling of the Hippo pathway, which has previously been described in connection with the pathogenesis of organ fibrosis, in which myofibroblasts participate through the production of fibrotic substance..[97]

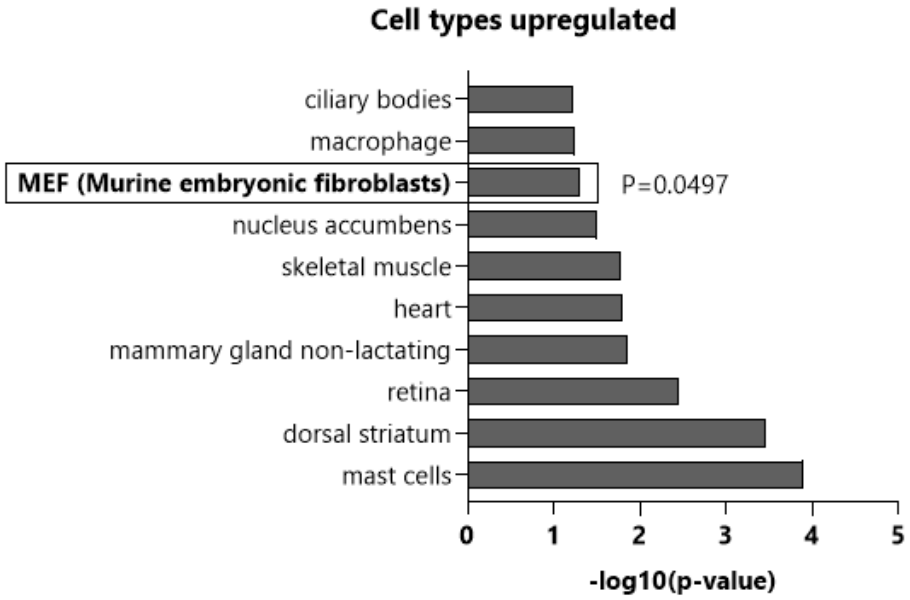

Figure 27: Pericytes in old hearts express fibroblast-related genes

Results of the GO analysis with Enrichr of the 244 downregulated and 92 upregulated DEG in old pericytes, classified in the top 10 cell types. Data are shown as negative logarithmic p-values.

4.3.2 *RGS5* knockdown leads to dedifferentiation of pericytes with loss of pericyte markers and expression of fibroblast markers

After this observation, we went back to our hBPV *in vitro* model and analysed the effect of *RGS5* knockdown on pericyte identity. RT-qPCR analysis of pericyte markers *PDGFRB* and *NOTCH3* revealed a reduced expression upon siRGS5 transfection. These observations lead us to consider that aging might induce an identity shift to the pericytes. Consistent with the observations in the snRNAseq analysis that showed a shift towards a fibroblast-like cell identity, hBVPs upregulate *COL1A1,* a marker for brain fibroblasts encoding another alpha chain of fibrillary collagen similar.[98]

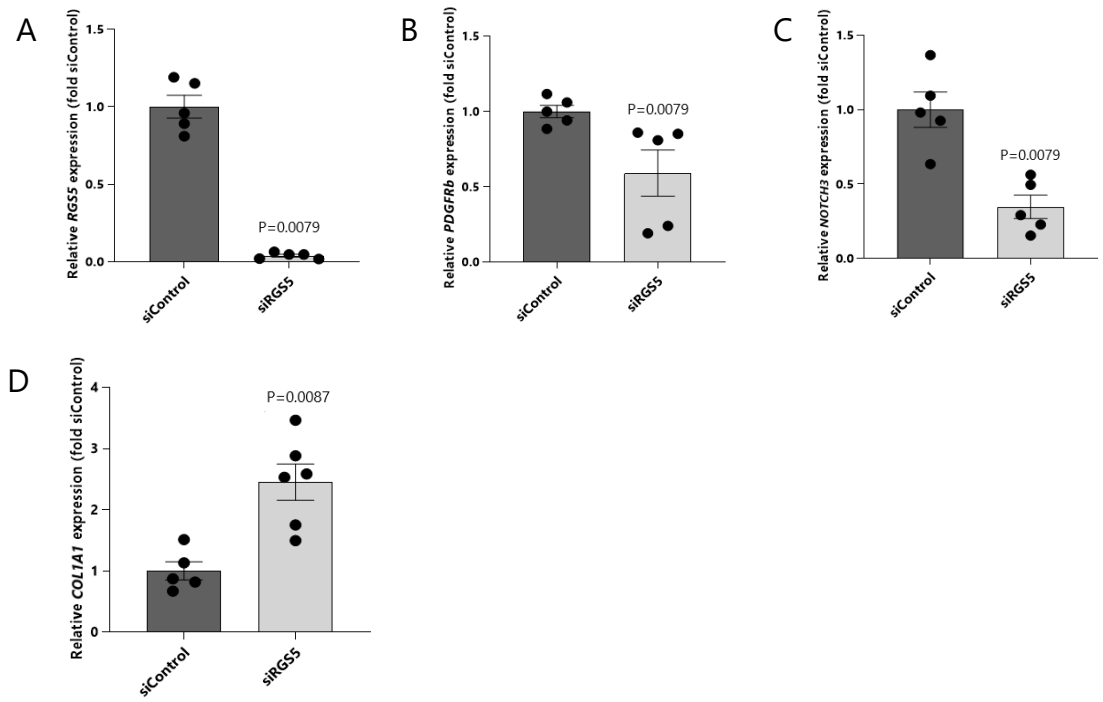

Figure 28: *RGS5* knockdown is enough to induce an identity change in hBVPs

Data show the mean ± SEM relative expression of (A) RGS5, (B) *PDGFRB*, (C) *NOTCH3 and (D) COL1A1* 48 hours after siRNA treatment of hBVPs. The measurement was done in independent experiments (N=5). Statistical analysis was performed using the nonparametric two-tailed Mann-Whitney test.

5 Discussion

Pericytes, like other mural cells, participate in various physiological and pathological processes throughout the microvasculature. They have been identified as crucial regulators of vascular stability and remodeling.[99] Nevertheless, the differences of pericytes in young and old hearts, the differences in their gene expression pattern during aging and the role of age-dependent regulated genes on pericyte function has not yet been investigated.

The present study provides new insights into the pericyte population of the aging heart and suggests that *RGS5* is required for pericyte adhesion to endothelial cells. Its downregulation in the aged mural cells could explain the reduction of pericyte coverage in the old hearts. Further, *RGS5* may be required to maintain pericyte identity.

5.1 Characterization of cardiac pericytes during aging

This study characterizes the pericyte population in the aging heart. The single-nucleus transcriptome data revealed the presence of two independent clusters of pericytes that were selected by their expression of *Pdgfrb* and *Ng2* (*Cspg4*) as molecular markers of pericytes. These clusters did not differ in the distribution between young and old hearts and it can only be speculated whether they are different types or activity states of pericytes. Although *Pdgfrb* and *Ng2* are defined as the two main markers to identify pericytes[100], there is still no cellular marker to precisely distinguish pericytes from other mural cells and that is expressed independently from cellular dynamics.[41]

5.2 Regulation of pericyte genes in the aging heart

Differential gene expression analysis identified over 300 genes that are regulated in pericytes in the aged heart. To further classify the biological functions of those differentially expressed genes, we performed a GO analysis. This revealed that

genes related to cellular focal adhesion contacts were downregulated in the aged pericytes. Involved genes in this category were, besides a variety of ribosomal proteins, Ras homolog family member A *(Rhoa*), mitogen-activated protein kinase kinase 1 *(Map2k1*), also known as MEK1, and actin beta (*Actb)*, which are all involved in the reorganization of the actin cytoskeleton by regulating the MAPK signalling cascade and, in this way, contribute to focal adhesion.[101] RHOA is a member of the family of small GTP-binding proteins, necessary for the formation of cell-matrix adhesion contacts and organization of the actin cytoskeleton, thereby controlling directive cell migration.[102] RHOA signaling is involved in vascular remodeling processes and the regulation of vSMC differentiation.[103,104] In pericytes, RHO GTPases have been described as modulators of their contractile phenotype and Rho-dependent signaling is relevant for the intercellular communication between pericytes and endothelial cells [105]

The reduction of focal adhesion contacts and the actin network due to a downregulation of RHOA may indicate the mechanism that is leading to the reduced density of pericytes in aging capillaries. Though RHOA is also involved in the regulation of migration, our data indicate that there is an upregulation of other migration-related genes in old pericytes that may compensate for the downregulation of RHOA. Those genes included *dmd* and *fgf13*. *Dmd* as well as *fgf13* were also upregulated in our single-nucleus transcriptome data concerning filopodium membrane and actin-based projection. Together, the categories of these upregulated genes in the GO analysis indicate an activation of the migratory potential of aging pericytes.

5.3 Regulation of pericyte function by *RGS5*

Our study identified *Rgs5* as one DEG downregulated in aged pericytes. We further confirmed the reduced expression of Rgs5 in the cardiac tissue of aging mice *in vivo*. RGS5 has been previously described as a marker of pericyte

identity[106] and modulates signaling pathways associated with regulatory processes in the vascular system.[107] Previous research investigated the relevance of Rgs5 for blood pressure regulation[67] and the development of different vascular diseases as myocardial infarction[108], cardiac hypertrophy[109] and atherosclerosis.[63]

To gain further understanding of the age-related alterations downstream the downregulation of *RGS5* in pericytes and to investigate if its downregulation would lead to a premature aging effect in pericytes, we performed a knockdown of *RGS5* in hBVP *in vitro*. We have used hBVP for our *in vitro* studies and although we are well aware that the conclusion that can be drawn from these studies might not be directly transferred to cardiac pericytes, they provide an excellent tool to study pericyte biology *in vitro*. The subsequent isolation and study of cardiac pericytes is a clear objective that emerges from this study. It will be crucial to gain greater insight into the role of pericytes in the heart.

In this work, the knockdown of *RGS5* in hBVP was not associated with crucial metabolic changes nor with impaired viability of the cells, suggesting that the knockdown affects other mechanisms more associated with the cellular function carried out by the pericytes in the heart. This could explain the reduction of pericyte coverage in the old hearts. Although the loss of pericytes is accompanied with an increased permeability of the microvasculature and edema formation in the retina[47], the knockdown of *RGS5* in pericytes had no effect to endothelial permeability. This may indicate that RGS5 does not participate in the molecular pathways underlying the regulation of cellular permeability or that pericytes are able to compensate for this effect through upregulation of supporting pathways.

To understand the mechanism of these pericyte-related changes in aging, we further analysed pericyte cellular adhesion *in vitro*. *RGS5* knockdown leads to detachment of pericytes both from a gelatin matrix and from endothelial cells

and is accompanied by the formation of filopodia-like structures that may refer to phenotypical alterations. This supports our hypothesis that the loss of pericytes in aging can be explained by a detachment of pericytes or a reduced adhesion capability of pericytes to endothelial cells of the microvasculature.

As previously introduced, aging pericytes present a downregulation of the GTPase Rho and subsequent signaling cascades that include MAPK and the actin skeleton. A correlation between RGS5 and the RHOA signaling pathway and the impairment of vascular remodeling processes has been described in other studies and may explain the underlying mechanism.[110]

Although the role of RGS5 in molecular signaling processes is not yet fully understood, there are indications that this protein is of great relevance for the regulation of cellular dynamics and the functioning of the vascular system.

5.4 Effect of RGS5 on pericyte identity

The phenotypical changes in the pericytes under *RGS5* knockdown led to the hypothesis that in addition to a change in the cytoskeleton and adhesion, a transition to another cell type might be part of the underlying mechanism. To test this hypothesis, we analysed the expression profile of different markers that are widely expressed in pericytes and fibroblasts. We show that upon *RGS5* knockdown pericytes show a shift in their profile of cellular markers, with a decrease of *PDGFRB* and *NOTCH3*, typical pericyte markers, and an increase of *COL1A1*, a fibroblast marker. This raises the hypothesis whether *RGS5* is required to maintain the identity of pericytes.

The relationship between *RGS5*, *PDGFRB* and *NOTCH3* has not yet been fully elucidated. The simultaneous downregulation of both markers, *PDGFRB* and *NOTCH3*, could indicate that their expression is downstream of *RGS5* activity. The

interaction between these signaling molecules could explain the altered behaviour of pericytes at the molecular level. It is known from previous work on retinas that PDGFRB and its ligand Platelet Derived Growth Factor Subunit B (PDGFB) play a role in the recruitment of pericytes to endothelial cells.[111] An impaired function resulting from the downregulation of *RGS5* would, therefore, lead to a loss of pericytes from capillaries. Correspondingly, the function of *NOTCH3* in pericytes is also not yet fully understood. In pericytes of zebrafish brains, *NOTCH3* plays a role in their proliferation and is thus presumably involved in the regulation of pericyte coverage and integrity of brain capillaries.[112] The understanding of these mechanisms needs to be further clarified in future work. Although studies with *Rgs5* knockout mice have already been conducted in relation to pericytes and their role in the brain[113], future work could investigate function of pericytes under *Rgs5* loss in the heart. For this purpose, a pericyte-specific knockout of Rgs5 would be an ideal tool to study Rgs5 loss-of-function *in vivo*.

The role of *RGS5* in cardiac pericytes and the general implications of pericyte biology on heart function have not yet been sufficiently investigated. In the heart tissue, a knockdown of *Rgs5* is associated with an increase in apoptosis of cardiomyocytes with subsequent scar formation.[114] Contrary to this, there is evidence that in brain capillaries the knockout of *Rgs5* leads to an increase in pericyte density providing protection against stroke.[115,116] The different effects of Rgs5 in the brain and heart could be explained by the tissue and organ specificity of pericytes and their different functions in these tissues. Another factor influencing these different regeneration mechanisms might be the role of pericytes as mesenchymal progenitor cells, whose multiple differentiation into cells of different lineages might have different effects on tissue regeneration[50] but it is important to take into account the different responses of these organs to ischemic damage. While the brain undergoes a process that is mainly

characterized by the activation and colonization of glial cells, namely astrocytes and microglia, and a strong neovascularization in the ischemic area[117], the ischemic heart is characterized by massive scarring that involves the participation of a variety of different fibroblast-like cells to replace the structure and mechanical integrity of the damaged myocardium.[118]

Other studies have observed an association between *Rgs5* knockout and increased fibrosis of the heart tissue.[65] Cardiac fibrosis occurs mainly after myocardial infarction and is defined as scarring with a pathological remodeling process of the extracellular matrix substance. This involves the activation of cardiac fibroblasts, which differentiate into myofibroblasts.[119] In this context, pericytes are also discussed as precursors of myofibroblasts, thereby contributing to the development of cardiac fibrosis.[120] Our observation of increased expression of the fibroblast marker *COL1A1*, the similarity between old cardiac pericytes and fibroblasts observed in the gene ontology analysis, as well as the phenotypical shift upon *RGS5* knockdown with filopodium formation could provide an explanation for the increase of cardiac fibrosis. Thereby, dedifferentiation of pericytes to fibroblasts might contribute to the development of fibrosis. RGS5 could be a key regulator for this pericyte dedifferentiation and a loss of RGS5 expression in aging could enhance the cardiac fibrosis. However, further work is still necessary in order to be able to understand the changes in cardiac pericytes.

5.5 Outlook

Within this study, we identified the loss of *Rgs5* as a characteristic of aged pericytes in the cardiac tissue. We furthermore studied its role in pericytes *in vitro*. Nevertheless, the molecular mechanisms downstream of the RGS5 loss-of-function remain unresolved. Further work is needed to analyse the effects on heart function both in homeostasis and in disease using *in vitro* experiments on isolated cardiac pericytes and an acute myocardial infarct model with pericyte-

specific *Rgs5* knock out mice *in vivo*. The relevance of the understanding of cardiac pericytes is also highlighted by the latest results of research on COVID-19, suggesting that pericytes, by specifically expressing the SARS-Cov-2 receptor ACE2, enable the virus to enter the vascular system, thus explaining the cause of severe disease progression.[121]

5.6 Conclusion

Age-related structural alterations of the heart are accompanied by the loss of pericytes. In the aging heart, pericytes present a different expression pattern. Due to the reduced expression of RGS5, pericytes lose the ability to adhere to endothelial cells and show an altered phenotype with formation of filopodia-like structures. The simultaneous loss of the pericyte markers PDGFRB and NOTCH3, as well as the overexpression of the fibroblast marker COL1A1, lead to the hypothesis that RGS5 is the key regulator for pericyte identity. The loss of RGS5 leads to the detachment of pericytes from the endothelium and the dedifferentiation to fibroblast-like cells. Together, this could explain cardiac remodeling processes that contribute to an increased fibrosis of the heart muscle during aging.

This work provides new insights into the function of pericytes in aging and presents a mechanism that might explain age-specific changes in the heart.

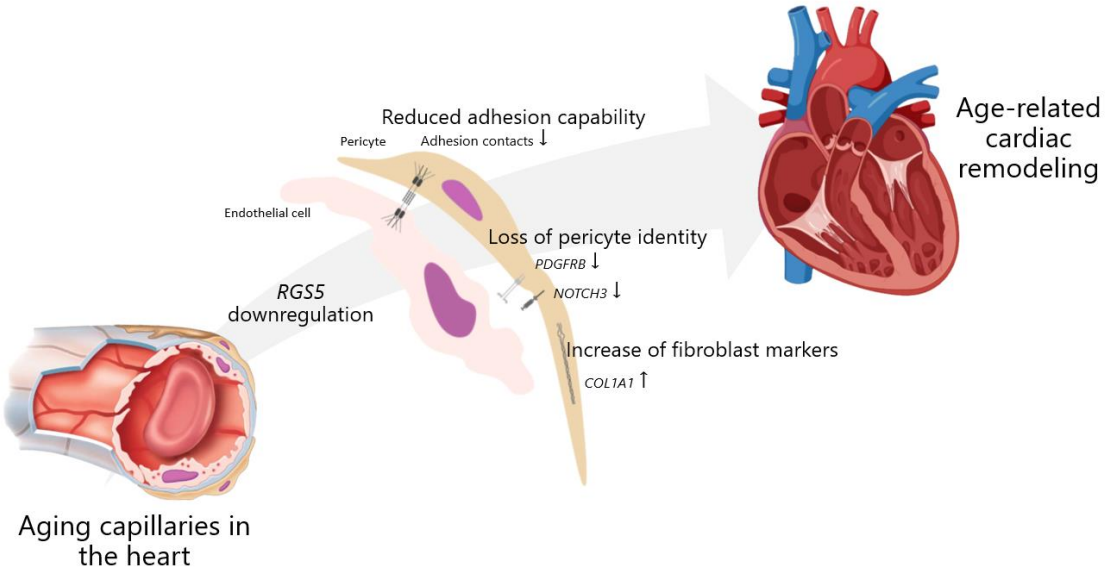

Figure 29: Role of *RGS5* downregulation in aging pericytes

RGS5 downregulation in aging capillaries affects adhesion capacity and pericyte identity. The latter may be due to impaired signaling via NOTCH3 and PDGFRB as well as the upregulation of fibroblast markers as shown for COL1A1. Together, these effects may contribute to alterations in cardiac remodeling.

Figure modified from Alcendor et al. 2019[40] and created with BioRender.com.

6 Summary

Cardiovascular disease (CVD) is the leading cause of death in the western world. Aging as the major risk factor for the development of CVD leads to structural changes in the heart and the vasculature. In addition to endothelial cells, mural cells, including smooth muscle cells and pericytes, form the vascular wall. Pericytes are defined as the perivascular cells located in the basement membrane of the capillaries, which are the smallest components of the vascular system and ensure the gas exchange in the tissue. In the different parts of the terminal vascular bed, pericytes receive different phenotypes and organ-specific functions. In addition to the stabilization of the vascular wall, pericytes are relevant for the formation of new vessels. Due to their potential of multipotent stem cells, pericytes can differentiate into different cell types and thus take a position in developmental processes. Pericytes play a crucial role in the development and diseases of the vascular system. Moreover, pericyte coverage is reduced in the aged heart. Nonetheless, the function of pericytes in the heart and their importance during cardiac aging is not completely understood.

To study the pericyte population in the aging heart, we have performed single-nucleus RNA-sequencing analysis comparing hearts from 12-weeks-old (young) and 18-month-old (old) mice. The detailed analysis of 336 differentially expressed genes (DEG) revealed that *Rgs5* is downregulated in aged pericytes. Regulator of G-protein signaling 5 (RGS5), an established marker for pericytes, is involved the regulation of the blood pressure and in the formation of various cardiovascular diesases, including cardiac hypertrophy, myocardial infarction and atherosclerosis. We have furthermore confirmed this observation *in vivo*. Gene ontology (GO) analysis of DEG revealed that aged pericytes are characterized by the downregulation of genes involved in cell adhesion. Further, we have performed cell biology approaches using human brain vascular pericytes (hBVP) to investigate the role of Rgs5 in pericytes *in vitro*. Efficient knockdown of *RGS5*,

although has no effect on cellular metabolism, viability and endothelial permeability, induces a reduction of pericyte adhesion to both a gelatine matrix and endothelial cells in a 3D matrigel culture. This was associated with the formation of filopodia. The altered phenotype suggested a changing identity of the pericytes. We could confirm that a loss of *RGS5* causes a decreased expression of the pericyte markers PDGFRb and NOTCH3 and also leads to an overexpression of COL1A1, a fibroblast marker.

Together, our findings suggest that RGS5 is required for pericyte adhesion to endothelial cells and its downregulation in the aged mural cells could explain the reduction of pericyte coverage in the aged hearts. Further, RGS5 may be the key regulator for pericyte identity, as pericytes show an altered expression profile of cellular markers. The dedifferentiation of pericytes to a more fibroblast-like cell type could explain the increased fibrosis during age-related cardiac remodeling. We believe that RGS5 is a great candidate to explore and study the molecular mechanisms that regulate pericyte function in the heart, both in homeostasis and during aging.

7 Zusammenfassung

Herz-Kreislauf-Erkrankungen sind die häufigste Todesursache in der westlichen Welt. Das Altern als Hauptrisikofaktor für deren Entstehung führt zu strukturellen Veränderungen im Herz und in den Gefäßen. Neben den Endothelzellen bilden murale Zellen, darunter glatte Muskelzellen und Perizyten, die Gefäßwand. Perizyten werden definiert als perivaskuläre Zellen, die sich in der Basalmembran der Kapillaren befinden, den kleinsten Bestandteilen des Gefäßsystems, die den Gasaustausch ins Gewebe gewährleisten. In den verschiedenen Teilen des terminalen Gefäßbetts besitzen Perizyten unterschiedliche Phänotypen und organspezifische Funktionen. Neben der Stabilisierung der Gefäßwand sind Perizyten auch für die Gefäßneubildung relevant. Aufgrund ihres Potenzials multipotenter Stammzellen können sich Perizyten in verschiedene Zelltypen differenzieren und so eine wichtige Rolle in Entwicklungsprozessen einnehmen. Sie sind entscheidend an der Entwicklung und Erkrankung des Gefäßsystems beteiligt. Zudem ist die Perizytenabdeckung der Gefäßwand im gealterten Herzen reduziert. Trotzdem ist die Funktion der Perizyten im Herzen und ihre Bedeutung bei der Alterung des Herzens noch nicht vollständig verstanden.

Um die Perizytenpopulation im alternden Herzen zu untersuchen, haben wir eine single-nucleus RNA-Sequenzierungsanalyse durchgeführt und dabei die Herzen von Mäusen im Alter von 12 Wochen (jungen) und 18 Monate (alten) miteinander verglichen. Die detaillierte Analyse von 336 differentiell exprimierten Genen (DEG) zeigte, dass *Rgs5* in gealterten Perizyten herunterreguliert wird. Der sogenannte *Regulator of G-protein signaling 5* (*RGS5*), ein etablierter Marker für Perizyten, ist an der Regulation des Blutdrucks und an der Entstehung verschiedener kardiovaskulärer Erkrankungen beteiligt, darunter Herzhypertrophie, Myokardinfarkt und Atherosklerose. Darüber hinaus haben wir diese Beobachtung *in vivo* bestätigt. Die Genontologieanalyse der DEG ergab, dass

gealterte Perizyten durch die Herunterregulierung von Genen gekennzeichnet sind, die an der Zelladhäsion beteiligt sind. Außerdem haben wir zellbiologische Versuche mit humanen Hirngefäßperizyten (hBVP) durchgeführt, um die Rolle von RGS5 in Perizyten *in vitro* zu untersuchen. Ein effizienter Knockdown von *RGS5* hat zwar keinen Einfluss auf den zellulären Metabolismus, die Lebensfähigkeit und die endotheliale Permeabilität, induziert jedoch eine Reduktion der Perizytenadhäsion sowohl an einer Gelatinematrix als auch an Endothelzellen in einer 3D-Matrigelkultur. Dies war mit der Bildung von Filopodien verbunden. Der veränderte Phänotyp deutete auf eine veränderte Identität der Perizyten hin. Wir konnten bestätigen, dass ein Verlust von RGS5 eine verminderte Expression der Perizytenmarker PDGFRB und NOTCH3 verursacht und darüber hinaus zu einer Überexpression von COL1A1, einem Fibroblastenmarker, führt.

Zusammenfassend deuten unsere Ergebnisse darauf hin, dass RGS5 für die Perizytenadhäsion an Endothelzellen erforderlich ist und seine Herunterregulierung in den gealterten muralen Zellen die Verminderung der Perizytenabdeckung in den gealterten Herzen erklären könnte. Darüber hinaus könnte Rgs5 der Schlüsselregulator für die Perizytenidentität sein, da Perizyten ein verändertes Expressionsprofil von zellulären Markern aufweisen. Die Dedifferenzierung der Perizyten zu einem eher Fibroblasten-ähnlichen Zelltyp könnte die erhöhte Fibrose während den altersbedingten kardialen Remodulierungsprozessen erklären. Wir glauben, dass RGS5 ein hervorragender Kandidat für die Erforschung und Untersuchung der molekularen Mechanismen ist, die die Perizytenfunktion im Herzen sowohl in der Homöostase als auch während des Alterns regulieren.

8 References

1. Benninghoff A, Drenckhahn D, Waschke J. *Taschenbuch Anatomie*. Urban & Fischer; 2014.
2. Aumüller G et al. Duale Reihe Anatomie. In: *Duale Reihe Anatomie*. Georg Thieme Verlag; 2010:118-128. doi:10.1055/b-0034-100799
3. Jin K. A Microcirculatory Theory of Aging. *Aging Dis*. 2019;10(3):676. doi:10.14336/ad.2019.0315
4. Marieb EN, Hoehn K. *Human Anatomy & Physiology*. Benjamin Cummings; 2010.
5. Lüllmann-Rauch R, ed. *Histologie*. Stuttgart: Georg Thieme Verlag; 2012. doi:10.1055/b-002-11390
6. Augustin HG, Koh GY. Organotypic vasculature: From descriptive heterogeneity to functional pathophysiology. *Science (80-)*. 2017;357(6353). doi:10.1126/science.aal2379
7. Holm A, Heumann T, Augustin HG. Microvascular Mural Cell Organotypic Heterogeneity and Functional Plasticity. *Trends Cell Biol*. 2018;28(4):302-316. doi:10.1016/j.tcb.2017.12.002
8. Drake RL, Vogl, Wayne A, Mitchell AWM. *Gray's Anatomy for Students, 2nd Edition*. Vol 2. Elsevier Health Sciences; 2009. doi:1437720552
9. Spencer JH, Anderson SE, Iaizzo PA. Human coronary venous anatomy: Implications for interventions. *J Cardiovasc Transl Res*. 2013;6(2):208-217. doi:10.1007/s12265-012-9443-y
10. Kirkwood TBL. Understanding the odd science of aging. *Cell*. 2005;120(4):437-447. doi:10.1016/j.cell.2005.01.027
11. McAuley MT, Guimera AM, Hodgson D, et al. Modelling the molecular mechanisms of aging. *Biosci Rep*. 2017;37(1). doi:10.1042/BSR20160177
12. North BJ, Sinclair DA. The intersection between aging and cardiovascular disease. *Circ Res*. 2012;110(8):1097-1108. doi:10.1161/CIRCRESAHA.111.246876
13. Lakatta EG, Levy D. Arterial and cardiac aging: Major shareholders in cardiovascular disease enterprises: Part I: Aging arteries: A "set up" for vascular disease. *Circulation*. 2003;107(1):139-146. doi:10.1161/01.CIR.0000048892.83521.58
14. Murtha LA, Schuliga MJ, Mabotuwana NS, et al. The processes and mechanisms of cardiac and pulmonary fibrosis. *Front Physiol*. 2017;8(OCT). doi:10.3389/fphys.2017.00777
15. Ferrari AU, Radaelli A, Centola M. Aging and the cardiovascular system. *J Appl Physiol*. 2003;95(6):2591-2597. doi:10.1152/japplphysiol.00601.2003
16. Virmani R, Avolio AP, Mergner WJ, et al. Effect of aging on aortic morphology in populations with high and low prevalence of hypertension and atherosclerosis: Comparison between occidental and Chinese communities. *Am J Pathol*. 1991;139(5):1119-1129.

17. Zieman SJ, Melenovsky V, Kass DA. Mechanisms, pathophysiology, and therapy of arterial stiffness. *Arterioscler Thromb Vasc Biol*. 2005;25(5):932-943. doi:10.1161/01.ATV.0000160548.78317.29
18. Michel JB. Circulating and cellular markers of endothelial dysfunction with aging in rats. *Am J Physiol - Hear Circ Physiol*. 1997;273(4 42-4). doi:10.1152/ajpheart.1997.273.4.h1941
19. Taddei S, Virdis A, Mattei P, et al. Aging and endothelial function in normotensive subjects and patients with essential hypertension. *Circulation*. 1995;91(7):1981-1987. doi:10.1161/01.CIR.91.7.1981
20. Vita JA, Treasure CB, Nabel EG, et al. Coronary vasomotor response to acetylcholine relates to risk factors for coronary artery disease. *Circulation*. 1990;81(2):491-497. doi:10.1161/01.CIR.81.2.491
21. Celermajer DS, Sorensen KE, Spiegelhalter DJ, Georgakopoulos D, Robinson J, Deanfield JE. Aging is associated with endothelial dysfunction in healthy men years before the age-related decline in women. *J Am Coll Cardiol*. 1994;24(2):471-476. doi:10.1016/0735-1097(94)90305-0
22. Van Der Heijden-Spek JJ, Staessen JA, Fagard RH, Hoeks AP, Struijker Boudier HA, Van Bortel LM. Effect of age on brachial artery wall properties differs from the aorta and is gender dependent: A population study. *Hypertension*. 2000;35(2):637-642. doi:10.1161/01.HYP.35.2.637
23. Aquaro GD, Cagnolo A, Tiwari KK, et al. Age-dependent changes in elastic properties of thoracic aorta evaluated by magnetic resonance in normal subjects. *Interact Cardiovasc Thorac Surg*. 2013;17(4):674. doi:10.1093/ICVTS/IVT261
24. Gerstenblith G, Frederiksen J, Yin FCP, Fortuin NJ, Lakatta EG, Weisfeldt ML. Echocardiographic assessment of a normal adult aging population. *Circulation*. 1977;56(2):273-278. doi:10.1161/01.CIR.56.2.273
25. Kuller LH, Lopez OL, MacKey RH, et al. Subclinical cardiovascular disease and death, dementia, and coronary heart disease in patients 80+ years. *J Am Coll Cardiol*. 2016;67(9):1013-1022. doi:10.1016/j.jacc.2015.12.034
26. Camici GG, Savarese G, Akhmedov A, Lüscher TF. Molecular mechanism of endothelial and vascular aging: Implications for cardiovascular disease. *Eur Heart J*. 2015;36(48):3392-3403. doi:10.1093/eurheartj/ehv587
27. Boyle AJ, Shih H, Hwang J, et al. Cardiomyopathy of aging in the mammalian heart is characterized by myocardial hypertrophy, fibrosis and a predisposition towards cardiomyocyte apoptosis and autophagy. *Exp Gerontol*. 2011;46(7):549-559. doi:10.1016/j.exger.2011.02.010
28. Koshy SKG, Reddy HK, Shukla HH. Collagen cross-linking: New dimension to cardiac remodeling. *Cardiovasc Res*. 2003;57(3):594-598. doi:10.1016/S0008-6363(02)00877-5
29. McLean MR, Bursztyn Goldberg P, Roberts J. An ultrastructural study of the effects of age on sympathetic innervation and atrial tissue in the rat. *J Mol Cell Cardiol*. 1983;15(2):75-92. doi:10.1016/0022-2828(83)90284-5

30. Scioli MG, Bielli A, Arcuri G, Ferlosio A, Orlandi A. Ageing and microvasculature. *Vasc Cell*. 2014;6(1):19. doi:10.1186/2045-824X-6-19
31. Van Der Loo B, Labugger R, Skepper JN, et al. Enhanced peroxynitrite formation is associated with vascular aging. *J Exp Med*. 2000;192(12):1731-1743. doi:10.1084/jem.192.12.1731
32. Förstermann U, Sessa WC. Nitric oxide synthases: Regulation and function. *Eur Heart J*. 2012;33(7):829-837. doi:10.1093/eurheartj/ehr304
33. Ferlosio A, Arcuri G, Doldo E, et al. Age-related increase of stem marker expression influences vascular smooth muscle cell properties. *Atherosclerosis*. 2012;224(1):51-57. doi:10.1016/j.atherosclerosis.2012.07.016
34. Lakatta EG. Cardiovascular regulatory mechanisms in advanced age. *Physiol Rev*. 1993;73(2):413-465. doi:10.1152/physrev.1993.73.2.413
35. Florey HW, Carleton HM. Rouget cells and their function. *Proc R Soc London Ser B, Contain Pap a Biol Character*. 1926;100(700):23-31. doi:10.1098/rspb.1926.0031
36. Zimmermann KW. Der feinere Bau der Blutcapillaren. *Z Anat Entwicklungsgesch*. 1923;68:3-109. doi:10.1007/bf02593544
37. Ribatti D, Nico B, Crivellato E. The role of pericytes in angiogenesis. *Int J Dev Biol*. 2011;55(3):261-268. doi:10.1387/ijdb.103167dr
38. Sweeney MD, Ayyadurai S, Zlokovic B V. Pericytes of the neurovascular unit: Key functions and signaling pathways. *Nat Neurosci*. 2016;19(6):771-783. doi:10.1038/nn.4288.Pericytes
39. Hartmann DA, Underly RG, Grant RI, Watson AN, Lindner V, Shih AY. Pericyte structure and distribution in the cerebral cortex revealed by high-resolution imaging of transgenic mice. *Neurophotonics*. 2015;2(4):041402. doi:10.1117/1.NPh.2.4.041402
40. Alcendor DJ. Human vascular pericytes and cytomegalovirus pathobiology. *Int J Mol Sci*. 2019;20(6):1456. doi:10.3390/ijms20061456
41. Armulik A, Genové G, Betsholtz C. Pericytes: Developmental, Physiological, and Pathological Perspectives, Problems, and Promises. *Dev Cell*. 2011;21(2):193-215. doi:10.1016/j.devcel.2011.07.001
42. Gaengel K, Genové G, Armulik A, Betsholtz C. Endothelial-mural cell signaling in vascular development and angiogenesis. *Arterioscler Thromb Vasc Biol*. 2009;29(5):630-638. doi:10.1161/ATVBAHA.107.161521
43. Hellstrom M, Kalen M, Lindahl P, Abramsson A, Betsholtz C. Role of PDGF-B and PDGFR-beta in recruitment of vascular smooth muscle cells and pericytes during embryonic blood vessel formation in the mouse. *Development*. 1999;126(14):3047-3055. doi:10.1186/1471-2148-8-34
44. Chen Q, Zhang H, Liu Y, et al. Endothelial cells are progenitors of cardiac pericytes and vascular smooth muscle cells. *Nat Commun*. 2016;7(1):1-13. doi:10.1038/ncomms12422
45. Volz KS, Jacobs AH, Chen HI, et al. Pericytes are progenitors for coronary

artery smooth muscle. *Elife*. 2015;4. doi:10.7554/eLife.10036
46. Majesky MW. Developmental basis of vascular smooth muscle diversity. *Arterioscler Thromb Vasc Biol*. 2007;27(6):1248-1258. doi:10.1161/ATVBAHA.107.141069
47. Bergers G, Song S. The role of pericytes in blood-vessel formation and maintenance. *Neuro Oncol*. 2005;7(4):452-464. doi:10.1215/s1152851705000232
48. Attwell D, Mishra A, Hall CN, O'Farrell FM, Dalkara T. What is a pericyte? *J Cereb Blood Flow Metab*. 2016;36(2):451-455. doi:10.1177/0271678X15610340
49. Nakagomi T, Kubo S, Nakano-Doi A, et al. Brain vascular pericytes following ischemia have multipotential stem cell activity to differentiate into neural and vascular lineage cells. *Stem Cells*. 2015;33(6):1962-1974. doi:10.1002/stem.1977
50. Scott RW, Arostegui M, Schweitzer R, Rossi FMV, Underhill TM. Hic1 Defines Quiescent Mesenchymal Progenitor Subpopulations with Distinct Functions and Fates in Skeletal Muscle Regeneration. *Cell Stem Cell*. 2019;25(6):797-813.e9. doi:10.1016/j.stem.2019.11.004
51. Hughes S, Gardiner T, Hu P, Baxter L, Rosinova E, Chan-Ling T. Altered pericyte-endothelial relations in the rat retina during aging: Implications for vessel stability. *Neurobiol Aging*. 2006;27(12):1838-1847. doi:10.1016/j.neurobiolaging.2005.10.021
52. Stewart PA, Magliocco M, Hayakawa K, et al. A quantitative analysis of blood-brain barrier ultrastructure in the aging human. *Microvasc Res*. 1987;33(2):270-282. doi:10.1016/0026-2862(87)90022-7
53. Kovacic JC, Moreno P, Nabel EG, Hachinski V, Fuster V. Cellular senescence, vascular disease, and aging: Part 2 of a 2-part review: Clinical vascular disease in the elderly. *Circulation*. 2011;123(17):1900-1910. doi:10.1161/CIRCULATIONAHA.110.009118
54. Alex L, Frangogiannis NG. Pericytes in the infarcted heart. 2019:H23-H31.
55. Kimple AJ, Bosch DE, Giguère PM, Siderovski DP. Regulators of G-protein signaling and their Gα substrates: Promises and challenges in their use as drug discovery targets. *Pharmacol Rev*. 2011;63(3):728-749. doi:10.1124/pr.110.003038
56. Manzur M, Ganss R. Regulator of G Protein Signaling 5: A New Player in Vascular Remodeling. *Trends Cardiovasc Med*. 2009;19(1):26-30. doi:10.1016/j.tcm.2009.04.002
57. Gunaje JJ, Bahrami AJ, Schwartz SM, Daum G, Mahoney WM. PDGF-dependent regulation of regulator of G protein signaling-5 expression and vascular smooth muscle cell functionality. *Am J Physiol Physiol*. 2011;301(2):C478-C489. doi:10.1152/ajpcell.00348.2010
58. Cho H, Kozasa T, Bondjers C, et al. Pericyte-specific expression of. *FASEB J*. 2003;(2).

59. Mitchell TS, Bradley J, Robinson GS, Shima DT, Ng YS. RGS5 expression is a quantitative measure of pericyte coverage of blood vessels. *Angiogenesis*. 2008;11(2):141-151. doi:10.1007/s10456-007-9085-x
60. CHO H, KOZASA T, BONDJERS C, BETSHOLTZ C, KEHRL JH. Pericyte-specific expression of Rgs5: implications for PDGF and EDG receptor signaling during vascular maturation. *FASEB J*. 2003;17(3):440-442. doi:10.1096/fj.02-0340fje
61. Berger M, Bergers G, Arnold B, Hämmerling GJ, Ganss R. Regulator of G-protein signaling-5 induction in pericytes coincides with active vessel remodeling during neovascularization. *Blood*. 2005;105(3):1094-1101. doi:10.1182/blood-2004-06-2315
62. Arnold C, Feldner A, Pfisterer L, et al. RGS5 promotes arterial growth during arteriogenesis. *EMBO Mol Med*. 2014;6(8):1075-1089. doi:10.15252/emmm.201403864
63. Cheng WL, Wang PX, Wang T, et al. Regulator of G-protein signalling 5 protects against atherosclerosis in apolipoprotein E-deficient mice. *Br J Pharmacol*. 2015;172(23):5676-5689. doi:10.1111/bph.12991
64. Li J, Adams LD, Wang X, et al. Regulator of G protein signaling 5 marks peripheral arterial smooth muscle cells and is downregulated in atherosclerotic plaque. *J Vasc Surg*. 2004;40(3):519-528. doi:10.1016/j.jvs.2004.06.021
65. Li H, He C, Feng J, Zhang Y. Regulator of G protein signaling 5 protects against cardiac hypertrophy and fibrosis duringbiomechanical stress of pressure overload. 2018;115(16).
66. Ding H-S, Huang Y, Chen Z, et al. Regulator of G-protein signalling 5 deficiency impairs ventricular remodelling after myocardial infarction by promoting NF-κB and MAPK signalling in mice. *Biochem Biophys Res Commun*. 2018;499(2):143-149. doi:10.1016/j.bbrc.2018.03.082
67. Holobotovskyy V, Manzur M, Tare M, et al. Regulator of G-protein signaling 5 controls blood pressure homeostasis and vessel wall remodeling. *Circ Res*. 2013;112(5):781-791. doi:10.1161/CIRCRESAHA.111.300142
68. Vidal R, Wagner JUG, Braeuning C, et al. Transcriptional heterogeneity of fibroblasts is a hallmark of the aging heart. *JCI Insight*. 2019;4(22). doi:10.1172/jci.insight.131092
69. Chen EY, Tan CM, Kou Y, et al. Enrichr: Interactive and collaborative HTML5 gene list enrichment analysis tool. *BMC Bioinformatics*. 2013;14. doi:10.1186/1471-2105-14-128
70. Kuleshov M V., Jones MR, Rouillard AD, et al. Enrichr: a comprehensive gene set enrichment analysis web server 2016 update. *Nucleic Acids Res*. 2016;44(W1):W90-W97. doi:10.1093/nar/gkw377
71. Wagner JUG, Pham MD, Nicin L, et al. Dissection of heterocellular cross-talk in vascularized cardiac tissue mimetics. *J Mol Cell Cardiol*.

2020;138:269-282. doi:10.1016/j.yjmcc.2019.12.005
72. Luxán G, Stewen J, Díaz N, et al. Endothelial EphB4 maintains vascular integrity and transport function in adult heart. *Elife*. 2019;8. doi:10.7554/eLife.45863
73. Ge B, Li J, Wei Z, Sun T, Song Y, Khan NU. Functional expression of CCL8 and its interaction with chemokine receptor CCR3. *BMC Immunol*. 2017;18(1):54. doi:10.1186/s12865-017-0237-5
74. Levy DE, Lee C. What does Stat3 do? *J Clin Invest*. 2002;109(9):1143-1148. doi:10.1172/jci15650
75. Jia C, Keasey MP, Malone HM, et al. Vitronectin from brain pericytes promotes adult forebrain neurogenesis by stimulating CNTF. *Exp Neurol*. 2019;312:20-32. doi:10.1016/j.expneurol.2018.11.002
76. Jansson D, Rustenhoven J, Feng S, et al. A role for human brain pericytes in neuroinflammation. *J Neuroinflammation*. 2014;11:104. doi:10.1186/1742-2094-11-104
77. Carlsson R, Özen I, Barbariga M, Gaceb A, Roth M, Paul G. STAT3 precedes HIF1α transcriptional responses to oxygen and oxygen and glucose deprivation in human brain pericytes. *PLoS One*. 2018;13(3). doi:10.1371/journal.pone.0194146
78. Nowak KJ, Davies KE. Duchenne muscular dystrophy and dystrophin: Pathogenesis and opportunities for treatment: Third in molecular medicine review series. *EMBO Rep*. 2004;5(9):872-876. doi:10.1038/sj.embor.7400221
79. Wu QF, Yang L, Li S, et al. Fibroblast growth factor 13 is a microtubule-stabilizing protein regulating neuronal polarization and migration. *Cell*. 2012;149(7):1549-1564. doi:10.1016/j.cell.2012.04.046
80. Hollern DP, Swiatnicki MR, Rennhack JP, et al. E2F1 Drives Breast Cancer Metastasis by Regulating the Target Gene FGF13 and Altering Cell Fax Running Title: Mechanism of E2F regulated breast cancer metastasis. *bioRxiv*. June 2019:671149. doi:10.1101/671149
81. Pratt JR, Basheer SA, Sacks SH. Local synthesis of complement component C3 regulates acute renal transplant rejection. *Nat Med*. 2002;8(6):582-587. doi:10.1038/nm0602-582
82. Silveira AC, Morrison MA, Ji F, et al. Convergence of linkage, gene expression and association data demonstrates the influence of the RAR-related orphan receptor alpha (RORA) gene on neovascular AMD: A systems biology based approach. *Vision Res*. 2010;50(7):698-715. doi:10.1016/j.visres.2009.09.016
83. Okada T, Keino-Masu K, Nagamine S, et al. Desulfation of Heparan Sulfate by Sulf1 and Sulf2 Is Required for Corticospinal Tract Formation. *Sci Rep*. 2017;7(1):1-14. doi:10.1038/s41598-017-14185-3
84. Mi H, Muruganujan A, Casagrande JT, Thomas PD. Large-scale gene function analysis with the panther classification system. *Nat Protoc*.

2013;8(8):1551-1566. doi:10.1038/nprot.2013.092
85. Wang W, Zhang W, Han Y, et al. NELIN, a new F-actin associated protein, stimulates HeLa cell migration and adhesion. *Biochem Biophys Res Commun*. 2005;330(4):1127-1131. doi:10.1016/j.bbrc.2005.03.082
86. Ohtsuka T, Nakanishi H, Ikeda W, et al. Nexilin: A novel actin filament-binding protein localized at cell- matrix adherens junction. *J Cell Biol*. 1998;143(5):1227-1238. doi:10.1083/jcb.143.5.1227
87. Pei C, Qin S, Wang M, Zhang S. Regulatory mechanism of human vascular smooth muscle cell phenotypic transformation induced by NELIN. *Mol Med Rep*. 2015;12(5):7310-7316. doi:10.3892/mmr.2015.4365
88. Zhu B, Rippe C, Holmberg J, et al. Nexilin/NEXN controls actin polymerization in smooth muscle and is regulated by myocardin family coactivators and YAP. *Sci Rep*. 2018;8(1):1-17. doi:10.1038/s41598-018-31328-2
89. Wu C, Yan H, Sun J, et al. NEXN is a novel susceptibility gene for coronary artery disease in Han Chinese. *PLoS One*. 2013;8(12). doi:10.1371/journal.pone.0082135
90. Laitinen L. Griffonia simplicifolia lectins bind specifically to endothelial cells and some epithelial cells in mouse tissues. *Histochem J*. 1987;19(4):225-234. doi:10.1007/BF01680633
91. Armulik A, Genové G, Mäe M, et al. Pericytes regulate the blood-brain barrier. *Nature*. 2010;468(7323):557-561. doi:10.1038/nature09522
92. Van Nieuw Amerongen GP, Draijer R, Vermeer MA, Van Hinsbergh VWM. Transient and prolonged increase in endothelial permeability induced by histamine and thrombin: Role of protein kinases, calcium, and RhoA. *Circ Res*. 1998;83(11):1115-1123. doi:10.1161/01.RES.83.11.1115
93. Hautbergue GM, Hung ML, Walsh MJ, et al. UIF, a New mRNA Export Adaptor that Works Together with REF/ALY, Requires FACT for Recruitment to mRNA. *Curr Biol*. 2009;19(22):1918-1924. doi:10.1016/j.cub.2009.09.041
94. Azuaje F, Zhang L, Jeanty C, Puhl SL, Rodius S, Wagner DR. Analysis of a gene co-expression network establishes robust association between Col5a2 and ischemic heart disease. *BMC Med Genomics*. 2013;6(1):13. doi:10.1186/1755-8794-6-13
95. Boam DSW, Davidson I, Chambon P. A TATA-less promoter containing binding sites for ubiquitous transcription factors mediates cell type-specific regulation of the gene for transcription enhancer factor-1 (TEF-1). *J Biol Chem*. 1995;270(33):19487-19494. doi:10.1074/jbc.270.33.19487
96. Zhang J, Tao R, Campbell KF, et al. Functional cardiac fibroblasts derived from human pluripotent stem cells via second heart field progenitors. *Nat Commun*. 2019;10(1):1-15. doi:10.1038/s41467-019-09831-5
97. Kim C, Choi S, Mo J. Role of the Hippo Pathway in Fibrosis and Cancer. 2019:1-22.

98. Vanlandewijck M, He L, Mäe MA, et al. A molecular atlas of cell types and zonation in the brain vasculature. *Nature*. 2018;554(7693):475-480. doi:10.1038/nature25739
99. Armulik A, Abramsson A, Betsholtz C. Endothelial/pericyte interactions. *Circ Res*. 2005;97(6):512-523. doi:10.1161/01.RES.0000182903.16652.d7
100. He L, Vanlandewijck M, Raschperger E, et al. Analysis of the brain mural cell transcriptome. *Sci Rep*. 2016;6. doi:10.1038/srep35108
101. Frost JA, Steen H, Shapiro P, et al. Cross-cascade activation of ERKs and ternary complex factors by Rho family proteins. *EMBO J*. 1997;16(21):6426-6438. doi:10.1093/emboj
102. Warner H, Wilson BJ, Caswell PT. Control of adhesion and protrusion in cell migration by Rho GTPases. *Curr Opin Cell Biol*. 2019;56:64-70. doi:10.1016/j.ceb.2018.09.003
103. Tang L, Dai F, Liu Y, et al. RhoA/ROCK signaling regulates smooth muscle phenotypic modulation and vascular remodeling via the JNK pathway and vimentin cytoskeleton. *Pharmacol Res*. 2018;133:201-212. doi:10.1016/j.phrs.2018.05.011
104. Althoff TF, Juárez JA, Troidl K, et al. Procontractile G protein-mediated signaling pathways antagonistically regulate smooth muscle differentiation in vascular remodeling. *J Exp Med*. 2012;209(12):2277-2290. doi:10.1084/jem.20120350
105. Kutcher ME, Kolyada AY, Surks HK, Herman IM. Pericyte Rho GTPase mediates both pericyte contractile phenotype and capillary endothelial growth state. *Am J Pathol*. 2007;171(2):693-701. doi:10.2353/ajpath.2007.070102
106. Mitchell TS, Bradley J, Robinson GS, Shima DT, Ng Y-S. RGS5 expression is a quantitative measure of pericyte coverage of blood vessels. *Angiogenesis*. 2008;11(2):141-151. doi:10.1007/s10456-007-9085-x
107. Manzur M, Ganss R. Regulator of G Protein Signaling 5: A New Player in Vascular Remodeling. *Trends Cardiovasc Med*. 2009;19(1):26-30. doi:10.1016/j.tcm.2009.04.002
108. Wang Z, Huang H, He W, et al. Regulator of G-protein signaling 5 protects cardiomyocytes against apoptosis during in vitro cardiac ischemia-reperfusion in mice by inhibiting both JNK1/2 and P38 signaling pathways. *Biochem Biophys Res Commun*. 2016;473(2):551-557. doi:10.1016/j.bbrc.2016.03.114
109. Ding H-S, Huang Y, Chen Z, et al. Regulator of G-protein signalling 5 deficiency impairs ventricular remodelling after myocardial infarction by promoting NF-κB and MAPK signalling in mice. *Biochem Biophys Res Commun*. 2018;499(2):143-149. doi:10.1016/j.bbrc.2018.03.082
110. Arnold C, Demirel E, Feldner A, et al. Hypertension-evoked RhoA activity in vascular smooth muscle cells requires RGS5. *FASEB J*. 2018;32(4):2021-2035. doi:10.1096/fj.201700384RR

111. Hammes HP. Pericytes and the pathogenesis of diabetic retinopathy. *Horm Metab Res*. 2005;37(SUPPL. 1):3107-3112. doi:10.1055/s-2005-861361
112. Wang YY, Pan LY, Moens CB, Appel B. Notch3 establishes brain vascular integrity by regulating pericyte number. *Dev*. 2014;141(2):307-317. doi:10.1242/dev.096107
113. Nisancioglu MH, Mahoney WM, Kimmel DD, Schwartz SM, Betsholtz C, Genove G. Generation and Characterization of rgs5 Mutant Mice. *Mol Cell Biol*. 2008;28(7):2324-2331. doi:10.1128/MCB.01252-07
114. Wang Z, Huang H, He W, et al. Regulator of G-protein signaling 5 protects cardiomyocytes against apoptosis during in vitro cardiac ischemia-reperfusion in mice by inhibiting both JNK1/2 and P38 signaling pathways. *Biochem Biophys Res Commun*. 2016;473(2):551-557. doi:10.1016/j.bbrc.2016.03.114
115. Roth M, Gaceb A, Enström A, et al. Regulator of G-protein signaling 5 regulates the shift from perivascular to parenchymal pericytes in the chronic phase after stroke. *FASEB J*. 2019;33(8):fj.201900153R. doi:10.1096/fj.201900153r
116. Özen I, Roth M, Barbariga M, et al. Loss of Regulator of G-Protein Signaling 5 Leads to Neurovascular Protection in Stroke. *Stroke*. 2018;49(9):2182-2190. doi:10.1161/STROKEAHA.118.020124
117. Buscemi L, Price M, Bezzi P, Hirt L. Spatio-temporal overview of neuroinflammation in an experimental mouse stroke model. *Sci Rep*. 2019;9(1). doi:10.1038/s41598-018-36598-4
118. Rog-Zielinska EA, Norris RA, Kohl P, Markwald R. The Living scar - cardiac fibroblasts and the injured heart. *Trends Mol Med*. 2016;22(2):99-114. doi:10.1016/j.molmed.2015.12.006
119. Hinderer S, Schenke-Layland K. Cardiac fibrosis – A short review of causes and therapeutic strategies. *Adv Drug Deliv Rev*. 2019;146:77-82. doi:10.1016/j.addr.2019.05.011
120. Greenhalgh SN, Iredale JP, Henderson NC. Origins of fibrosis: Pericytes take centre stage. *F1000Prime Rep*. 2013;5. doi:10.12703/P5-37
121. He L, Mäe MA, Sun Y, et al. Pericyte-specific vascular expression of SARS-CoV-2 receptor ACE2 – implications for microvascular inflammation and hypercoagulopathy in COVID-19 patients. *bioRxiv*. May 2020:2020.05.11.088500. doi:10.1101/2020.05.11.088500

9 Acknowledgement

10 Schriftliche Erklärung

Ich erkläre ehrenwörtlich, dass ich die dem Fachbereich Medizin der Johann Wolfgang Goethe-Universität Frankfurt am Main zur Promotionsprüfung eingereichte Dissertation mit dem Titel

The role of *RGS5* downregulation in pericytes of the aging heart

im Institut für Kardiovaskuläre Regeneration unter Betreuung und Anleitung von Prof. Dr. Stefanie Dimmeler mit Unterstützung durch Dr. Guillermo Luxán ohne sonstige Hilfe selbst durchgeführt und bei der Abfassung der Arbeit keine anderen als die in der Dissertation angeführten Hilfsmittel benutzt habe. Darüber hinaus versichere ich, nicht die Hilfe einer kommerziellen Promotionsvermittlung in Anspruch genommen zu haben.

Ich habe bisher an keiner in- oder ausländischen Universität ein Gesuch um Zulassung zur Promotion eingereicht*. Die vorliegende Arbeit wurde bisher nicht als Dissertation eingereicht.

Vorliegende Ergebnisse der Arbeit wurden (oder werden) in folgendem Publikationsorgan veröffentlicht:
[Auflistung aller Autoren der Reihenfolge nach, Titel, Zeitschrift, Band, Seite, Veröffentlichungsjahr]

_____ _____

(Ort, Datum) (Unterschrift)

*) im Falle des Nichtzutreffens entfernen